

Entanglement distillation based on Hamiltonian dynamics

Zitai Xu^{1,*} and Guoding Liu^{2,†}

¹*Joint Center for Quantum Information and Computer Science,
University of Maryland, College Park, Maryland 20742, USA*

²*Center for Quantum Information, Institute for Interdisciplinary
Information Sciences, Tsinghua University, Beijing, 100084 China*

Efficient entanglement distillation is a central task in quantum information science and future quantum networks. At the core of distillation protocols are the quantum error correction and detection schemes which enhance the fidelity of entangled pairs. Conventional protocols focus on digital systems, which typically require complicated compiled circuits, high-fidelity multi-qubit operations and delicate pulse-level control that impose high demands on near-term hardware. Crucially, the leading physical platforms for quantum networks, trapped ions and neutral atoms, are governed by native many-body Hamiltonians inherently suited for analog, continuous-time evolution. Adopting these natural dynamics is simpler than engineering digital logic via delicate pulse-level control. Motivated by this experimental reality, we seek to leverage the intrinsic analog capabilities for efficient entanglement distillation. In this work, we introduce the Hamiltonian entanglement distillation protocol, which exploits the intrinsic information scrambling generated by random time evolution under native Hamiltonians. We establish a quantitative connection between output fidelity and Out-of-Time-Order Correlators, showing that efficient scrambling directly implies good distillation performance. Since generic Hamiltonians are naturally efficient scramblers, the capability for distillation is ubiquitous: almost all Hamiltonians in the Hilbert space suffice for high-fidelity distillation. Numerical simulations of representative Rydberg-atom and trapped-ion systems further confirm that robust performance could be achieved using only short-range interactions and evolution times feasible in current experiments. By avoiding the complexity of digital circuit control, our approach substantially relaxes experimental requirements, providing a scalable route to entanglement engineering on current analog quantum platforms.

CONTENTS

I. Introduction	2
II. Hamiltonian-based distillation protocol	3
III. Error detection via Hamiltonian twirling	4
IV. Noise Tolerance	6
V. Simulation	7
A. Performance of Device-native Hamiltonian	7
B. Non-Pauli Noises	10
C. Noise Tolerance	10
VI. Outlook	11
Acknowledgments	12
References	12
A. Preliminary	15
1. Basic notations and quantities	15
2. Entanglement distillation	17
a. One-way hashing method.	17
b. Recurrence method.	17

* zt3927@umd.edu

† lgd22@mails.tsinghua.edu.cn

3. Twirling	18
4. Out-of-Time-Order Correlator	19
B. Some proofs	20
1. Proof of Theorem 1	20
2. Proof of Lemma 1	22
3. Proof of Theorem 2	22
4. Proof of Theorem 3	28
5. Proof of Theorem 4	30
C. Simulation setup for quantum key distribution and repeaters	32

I. INTRODUCTION

Quantum information processing promises a new era of computation and communication, with potential application like secure communication [1, 2], distributed computing [3–5], quantum simulation and enhanced sensing [6]. At the heart of many of these applications lies the prerequisite of shared entanglement, the nonlocal resource that makes quantum protocols fundamentally different from classical counterparts.

Despite its central role, entanglement is inherently fragile and susceptible to errors arising from imperfect operations and environmental noise, especially when we want to distribute entanglement between two remote parties. Consequently, raw shared entanglement often suffers from low fidelity and cannot be used directly. To address this, one must employ entanglement distillation, a process that extracts high-fidelity pairs from noisy ensembles. Realizing efficient protocols for this task is crucial yet challenging, requiring joint efforts in both theoretical protocol design and experimental implementation.

On the theoretical front, the field has seen extensive development. Since the seminal work establishing the link between distillation and quantum error correction [7], a wide variety of protocols have been proposed [8–14]. Most of these works leverage the stabilizer formalism for error detection or correction, employing high-performance codes to achieve strong distillation performance. In contrast, experimental realization lags behind these theoretical advances. Current implementations are restricted to elementary protocols like the 2-to-1 recurrence protocol [7] to demonstrate the basic principle [15–19]. This technological gap exists because while high-performance distillation protocols typically require high-weight measurements, multi-qubit gate operations, complex circuit compilation, and precise pulse-level control, even state-of-the-art experimental platforms [20] have not yet achieved these capabilities at the required scale and fidelity. What current experiments can reliably realize is limited to the smallest examples, such as the [2,1,2] code for recurrence protocols. Consequently, there is still a need for practically efficient protocols that can achieve high-fidelity distillation within the constraints of current experimental technology.

In this work, we resort to Hamiltonian dynamics in analog system to relax the high resource demands. Importantly, native analog evolution is a natural feature of the physical platforms currently leading the development of quantum networks: trapped ions and neutral atoms. While these platforms can be engineered to perform digital logic through complex compilation and fine-tuned pulse sequence [21], their native many-body Hamiltonians drive continuous-time analog evolution [22–24]. Exploiting such intrinsic evolution relaxes experimental demands while preserving the good scrambling power needed for a wide range of quantum tasks. Indeed, these analog dynamics have already proven useful in quantum learning protocols such as shadow tomography [25, 26]. These findings lead to the core problem of this work: Can the intrinsic Hamiltonian dynamics of analog quantum simulators be effectively harnessed for high-performance entanglement distillation? Furthermore, can we establish a quantitative connection between the specific Hamiltonian evolution and the distillation performance?

We answer these questions affirmatively by explicitly introducing a Hamiltonian entanglement distillation protocol. We then present a comprehensive analysis that proceeds from the theoretical foundations of scrambling-based distillation to its practical implementation on near-term devices. Theoretically, we directly builds a quantitative relationship between Out-of-Time-Order Correlator, a physical quantity regarding scrambling power of Hamiltonians, and the fidelity and yield of the distillation protocol, showing that strong scrambling directly implies high output fidelity. Since for generic family of Hamiltonians, the error scrambling power is strong, our result directly shows that the good distillation performance property is ubiquitous: almost all Hamiltonians in the Hilbert space exhibit sufficiently good scrambling power for high-fidelity distillation. Another relevant metric for distillation protocol is its noise tolerance in the extremely high noise region. We show that the Hamiltonian-based scheme suffice to saturate the theoretical 33.3% error-rate upper bound. Practically, we perform simulations on representative device-native Hamiltonians such as the Rydberg Hamiltonian and trapped-ion Hamiltonian to confirm that within experimentally feasible short time and qubit scale, these Hamiltonian could guarantee strong fidelity performance. In addition, we also demonstrate the

noise tolerance of our protocol in practical applications including repeaters and quantum key distribution, obtaining better maximal distances. We believe these findings represent a significant advance in analog quantum simulation and entanglement distillation, with considerable potential for near-term applications.

The structure of this paper is as follows. In Section II, we introduce the Hamiltonian entanglement distillation scheme and provide the intuition for why Hamiltonian dynamics serve as a suitable candidate for this task. In Section III, we present our main results, establishing a connection between the out-of-time-order correlators, output fidelity and yield, demonstrating that general Hamiltonians possess strong error-detection capabilities. In Section IV, we show that our protocol can saturate the noise-tolerance bound for local depolarizing noise. Section V presents numerical simulations that illustrate the practicality of our approach on mainstream quantum platforms. Finally, Section VI concludes with a discussion of our results and directions for future research.

II. HAMILTONIAN-BASED DISTILLATION PROTOCOL

The entanglement distillation task for two remote parties Alice and Bob, who share n noisy EPR pairs $\tilde{\rho}_{AB}$, is to do some local operations and classical communications to obtain fewer pairs of states with higher fidelity. To see how Hamiltonian dynamics could be leveraged in this process, we first define a Hamiltonian twirling channel \mathcal{N}_H as the ensemble average of the unitary evolution generated by H over a random interaction time:

Definition 1. Given a Hamiltonian H on Hilbert space \mathcal{H} and a time ensemble μ , we define the Hamiltonian twirling channel \mathcal{N}_H of a bipartite system $\mathcal{H}_{AB} = \mathcal{H}^{\otimes 2}$ as,

$$\mathcal{N}_H(\rho_{AB}) = \int_t (e^{-iHt} \otimes e^{iH^*t}) \rho_{AB} (e^{-iHt} \otimes e^{iH^*t})^\dagger \mu(t). \quad (1)$$

By construction, \mathcal{N}_H preserves the maximally entangled state. Specifically, for an n -qubit Hamiltonian H , one has $\mathcal{N}_H(|\Phi^+\rangle\langle\Phi^+|^{\otimes n}) = |\Phi^+\rangle\langle\Phi^+|^{\otimes n}$. This follows from the fact that, for any n -qubit unitary U , the maximally entangled state $|\Phi^+\rangle_{AB}^{\otimes n}$ is invariant under the bilateral action $U \otimes U^*$. That is, $(U_A \otimes U_B^*) |\Phi^+\rangle_{AB}^{\otimes n} = |\Phi^+\rangle_{AB}^{\otimes n}$, where the subscript of U denotes which party it is acting on and U^* denotes the complex conjugate of U .

Intuitively, evolving a fixed Hamiltonian for a random time scrambles local errors that do not commute with the Hamiltonian, effectively transforming them into global noise while leaving the EPR state invariant. This approach is reminiscent of the adding noise strategy in two-way entanglement distillation [27]. Although the average bit error rate and phase error rate may increase after applying the Hamiltonian twirling \mathcal{N}_H , the correlations between the noisy state and the environment are further decoupled. Consequently, when \mathcal{N}_H is augmented with an error-detection scheme [14], the noisy components can be identified and discarded with high efficiency, yielding EPR pairs with higher fidelity. Motivated by these observations, we introduce the following Hamiltonian-based in Box 1:

Box 1: Hamiltonian entanglement distillation protocol

- (1) Grouping: Alice and Bob select an n -qubit Hamiltonian H compatible with their devices. Suppose they share kn noisy EPR pairs. They partition these pairs into k groups ρ_1, \dots, ρ_k , each consisting of n EPR pairs.
- (2) Pauli twirling: For each group, Alice and Bob jointly sample a Pauli operator P from the n -qubit Pauli group and apply $P \otimes P^*$ to their respective subsystems, obtaining $\rho'_i = (P \otimes P^*) \rho_i (P \otimes P^*)$.
- (3) Hamiltonian twirling: For each group, Alice and Bob jointly sample a time t from time ensemble μ and simultaneously evolve under H and $-H^*$ on their respective subsystems for time t , producing $\rho''_i = (e^{-iHt} \otimes e^{iH^*t}) \rho'_i (e^{-iHt} \otimes e^{iH^*t})^\dagger$.
- (4) Error detection: Alice and Bob agree on a POVM M acting on m qubit pairs. For each group, they randomly select m pairs and apply the POVM. The group is kept if the two parties obtain identical measurement outcomes, otherwise, it is discarded.
- (5) Output: The surviving qubits form EPR pairs with enhanced fidelity, which can be used directly or passed to a subsequent one-way hashing error-correction protocol.

Several notes regarding the scheme are as follows. First, the reason why Alice and Bob performs a random Pauli and its conjugate to their system is basically for analysis simplicity because it turns the noise channel for EPR states into Pauli channel [7]. This is the most basic and cheap operations and even manageable in many analog simulators. And if, in reality, some analog simulators are not able to perform any Pauli gates, we can omit this step and the protocol should still give good performance as shown in simulation in Sec VB. Second, later on in this paper, for theoretical simplicity,

we will assume that the Hamiltonian satisfies two properties. First, it is non-degenerate. That is, all its eigenvalues are distinct. Second, the eigenvalues satisfy the non-degenerate gap condition, i.e. $\lambda_i - \lambda_j = \lambda_k - \lambda_l$ implies $(i, j) = (k, l)$. These assumptions are adopted for analytical simplicity. In practice, Hamiltonians with spectral degeneracies, such as the transverse-field Ising Hamiltonian, can also exhibit good performance, as demonstrated numerically in Sec. V. We also assume the time measure μ to be the Fourier transform of delta function δ , which gives the property that $\int_0^T e^{ixt} \mu(t) dt = 1_{x=0}$. In practice this can be approximated by randomly selecting t in an experimental friendly time range $[0, T]$. Third, the protocol requires the ability to implement a given Hamiltonian and its time-reversed evolution. This capability has been demonstrated in analog quantum simulators such as trapped-ion systems [28, 29]. For Hamiltonians that lack a natural inversion, the effective sign flip can often be achieved using simple local Pauli conjugations [30]. Fourth, the choice of measurement POVM M depends on the chosen Hamiltonian H . However, for most Hamiltonians, measuring m pairs in the computational basis suffices. Choosing a larger value of m can increase the fidelity of the retained states, but generally reduces the yield. Finally, additional error-correction steps may be applied after the protocol to further enhance performance. For instance, when the distilled entangled states are used for quantum key distribution, standard one-way hashing protocols [7] can be employed to extract secret keys via classical post-processing. However, such one-way error correction typically relies on large CSS codes, whose coherent implementation remains experimentally challenging on current platforms. As a result, except in quantum key distribution settings, error correction is rarely applied in present-day experiments.

It worth noting that for entanglement distillation the specific targets vary between theoretical and practical contexts. Theoretical studies typically focus on the asymptotic yield of perfect EPR pairs, whereas practical applications often require only that the state fidelity exceeds a certain threshold. Relevant targets include $F > 2/3$ for quantum teleportation [31, 32], $F > 1/\sqrt{2} \approx 0.71$ for violating Bell inequalities [33] and $F \gtrsim 0.9$ for distributed quantum networks [34]. Despite this distinction, efficient error detection serves as an important step for both ends. In practical scenarios, a single round of error detection is often sufficient to meet fidelity targets, without resorting to the more resource-intensive one-way correction. In theoretical studies, stronger error detection can improve overall performance in high-noise regimes, where it helps suppress errors before subsequent one-way error correction is applied. Motivated by this unifying role, we first focus on analyzing the performance of the error-detection step itself, deriving results that are directly relevant to both near-term experiments and theoretical studies in the next section.

III. ERROR DETECTION VIA HAMILTONIAN TWIRLING

The error-detection step is central to the performance of the protocol. In the ideal limit, where all errors are perfectly detected and discarded, the remaining states are pure EPR pairs. More generally, more effective error detection leads to improved distillation performance. In the Hamiltonian based entanglement distillation protocol, the error detection is achieved through information scrambling. When the evolution effectively transforms local errors into global noise, measuring a relatively small number m of qubits is sufficient to detect the noise with high probability, which would allow for high output fidelity. In this section, we formalize this intuition by establishing a quantitative connection between distillation performance and scrambling power, as characterized by out-of-time-order correlators (OTOCs). We further show that, for generic Hamiltonians, their intrinsic scrambling properties are sufficient to guarantee strong distillation performance.

To build intuition, we first consider the simplest case where the Hamiltonian is diagonal, $H_d = \text{diag}\{\lambda_1, \dots, \lambda_d\}$ and investigate how different errors behave under such Hamiltonian twirling and how efficiently they can be detected. In this setting, for a bipartite state ρ , we can observe that:

$$\mathcal{N}_{H_d}(\rho) = \sum_{i \neq j} (\rho_{ii,jj} |ii\rangle\langle jj| + \rho_{ij,ij} |ij\rangle\langle ij|) + \sum_i \rho_{ii,ii} |ii\rangle\langle ii|. \quad (2)$$

This equation shows that only the diagonal components and the off-diagonal terms $\rho_{ii,jj}$ survive. Notably, the terms $\rho_{ii,jj}$ are exactly the off-diagonal terms of EPR states $|\Phi^\pm\rangle\langle\Phi^\pm|$, whereas the off-diagonal terms of $|\Psi^\pm\rangle\langle\Psi^\pm|$ vanish. Consequently, under diagonal Hamiltonian twirling, any error containing an X -type component leads to complete decoherence. We formalize this observation in the following theorem.

Theorem 1. *Let Alice and Bob share n noisy EPR pairs of the form $|\psi\rangle = (P \otimes I) |\Phi^+\rangle_{AB}^{\otimes n}$, where a Pauli error $P = X_0 Z_0$ acts on Alice's subsystem, with X_0 and Z_0 denoting tensor products of single-qubit Pauli X and Z operators, respectively. Let \mathcal{N}_{H_d} denote the Hamiltonian twirling channel induced by the diagonal Hamiltonian H_d . If $X_0 \neq I$, then the output state after twirling is*

$$\mathcal{N}_{H_d}\left((P \otimes I) |\Phi^+\rangle\langle\Phi^+|^{\otimes n} (P \otimes I)\right) = (X_0 \otimes I) \Delta\left(|\Phi^+\rangle\langle\Phi^+|^{\otimes n}\right) (X_0 \otimes I), \quad (3)$$

where $\Delta(\cdot)$ denotes the global dephasing channel that removes all off-diagonal terms in the computational basis. If otherwise $X_0 = I$, then the state is invariant under twirling:

$$\mathcal{N}_{H_d}\left((P \otimes I)|\Phi^+\rangle\langle\Phi^+|^{\otimes n}(P \otimes I)\right) = (Z_0 \otimes I)|\Phi^+\rangle\langle\Phi^+|^{\otimes n}(Z_0 \otimes I). \quad (4)$$

This theorem shows that, under diagonal Hamiltonian twirling, any bit-flip error induces a global complete dephasing channel, whereas phase errors remain unattended. Since the complete dephasing channel Δ can be expressed as $\Delta(\rho) = \sum_{P \in \{I, Z\}^{\otimes n}} P \rho P$, measuring m qubits in the Hadamard basis yields identical outcomes for Alice and Bob with probability only 2^{-m} . Consequently, bit-flip errors are detected and suppressed exponentially, and the residual noise on the remaining $n - m$ pairs is almost exclusively Z -type.

The above example suggests a general intuition: errors that do not commute with the Hamiltonian are scrambled by the evolution and can therefore be efficiently detected and suppressed. To extend this picture beyond diagonal Hamiltonians, we must rigorously quantify the dynamical consequences of this non-commutativity. A natural physical quantity for this purpose is the OTOC, defined for two operators V and W under unitary evolution $U(t) = e^{-iHt}$ as

$$\text{OTOC}_{V,W}^{U(t)} = \frac{1}{d} \text{Tr}(\tilde{V}^\dagger W^\dagger \tilde{V} W), \quad (5)$$

where $\tilde{V} = U^\dagger(t)VU(t)$. We add a normalization factor $1/d$ here with d is the Hilbert space dimension such that for commuting Pauli operators OTOC can be normalized to 1. The decay of the OTOC over time quantifies the speed at which local information is scrambled into global information. In the following, we establishes the relationship between average OTOC of a Hamiltonian and the output fidelity, yield of the distillation protocols.

Lemma 1. *Consider a Hamiltonian distillation protocol for n noisy EPR pairs $\Lambda(|\Phi^+\rangle\langle\Phi^+|^{\otimes n})$ subject to Pauli noise $\Lambda(\rho) = \sum_{P \in \mathcal{P}} c_P P \rho P$ on Alice's system. Hamiltonian H together with a time ensemble μ is adopted to produce the channel \mathcal{N}_H in the twirling step. Error detection is implemented by Alice measuring a POVM $M = \{M_x\}$ and Bob measuring the conjugate $M^* = \{M_x^*\}$ on m qubits, chosen such that $\sum_x \text{Tr}(M_x \otimes M_x^* |\Phi^+\rangle\langle\Phi^+|^{\otimes n}) = 1$. The outcome corresponding to $I - \sum_x M_x \otimes M_x^*$ is interpreted as detected error and discarded. After post-selection, the output fidelity f_{output} and yield Y are given by*

$$f_{\text{output}} = \frac{1}{1 + \text{OTOC}_{\Lambda, M}^{\mathcal{N}_H}/c_I}, \quad (6)$$

$$Y = (c_I + \text{OTOC}_{\Lambda, M}^{\mathcal{N}_H})(1 - m/n).$$

Here c_I is the probability of obtaining identity channel in noise Λ . The averaged OTOC is defined as

$$\text{OTOC}_{\Lambda, M}^{\mathcal{N}_H} = \int_t \sum_{P \in \mathcal{P} \setminus I} \sum_x c_P \text{OTOC}_{P, M_x}^{e^{-iHt}} \cdot \mu(t). \quad (7)$$

This theorem shows that lower averaged OTOC leads to higher output fidelity. The behavior of the yield is more subtle. While reducing the averaged OTOC alone tends to decrease the it, the yield also depends explicitly on the number of measured qubits m . Crucially, for Hamiltonians with stronger scrambling capability, the same low averaged OTOC can be achieved with a smaller measurement size m . This reduction in m compensates for the OTOC-induced decrease in yield. Consequently, Hamiltonians with strong scrambling power remain favorable choices for the distillation protocol.

Strong scrambling, actually, is not a fine-tuned property but rather generic in large Hilbert spaces, suggesting that good distillation performance should be typical for a broad class of Hamiltonians. To make this statement precise, we consider the spectral decomposition $H = UDU^\dagger$, where D is diagonal and satisfies the non-degenerate eigenvalue and gap conditions, and U is the diagonalizing unitary. The most general U could be taken from the Haar random and we show that the average of this Haar random ensemble is good. The most general U comes from Haar measure. The next theorem shows that the average performance of U from Haar measure is good. Treating U as a generic unitary drawn from the Haar measure, we show in the next theorem that these general Hamiltonians lead to favorable distillation performance.

Theorem 2. *Consider a Hamiltonian distillation protocol for n noisy EPR pairs $\Lambda(|\Phi^+\rangle\langle\Phi^+|^{\otimes n})$ subject to Pauli noise $\Lambda(\rho) = \sum_{P \in \mathcal{P}} c_P P \rho P$ on Alice's system, with probability of identity channel being c_I . Consider a n -qubit Hamiltonian be $H = UDU^\dagger$, where U is drawn from the Haar measure in the twirling step. After Hamiltonian twirling with H and measuring m qubit pairs in the computational basis, the output fidelity and yield converge, in the large n limit, to*

$$f_{\text{out}} = \frac{c_I}{c_I + 2^{-m}(1 - c_I)}, \quad (8)$$

$$Y = (c_I(1 - 2^{-m}) + 2^{-m})(1 - m/n).$$

This theorem shows that generic Hamiltonians yield asymptotically high-performance distillation. In particular, measuring $O(n)$ qubits suffices to suppress errors exponentially. For example, under local i.i.d. noise models with noise strength below a certain threshold, the protocol achieves an output fidelity exponentially close to 1.

Note that in this theorem we adopt measurements in the computational basis. This choice is sufficient for generic Hamiltonians because, in high-dimensional Hilbert spaces, two arbitrarily chosen bases are overwhelmingly likely to be close to mutually unbiased [35]. Hamiltonian twirling decoheres the noisy state in the eigenbasis of H . When the resulting state is measured in a basis that is mutually unbiased to this eigenbasis, the measurement outcomes are uniformly random, and the probability that Alice and Bob obtain identical outcomes is therefore exponentially small. Since the computational basis is almost mutually unbiased with the eigenbasis of a generic Hamiltonian, it guarantees effective error detection and hence good distillation performance.

We conclude this section by considering a more structured class of Hamiltonians admitting a spectral decomposition of the form $H = CDC^\dagger$, where C belongs to the Clifford group. Such Hamiltonians are frustration free and can be written as sums of mutually commuting Pauli operators, $H_c = \sum_i c_i P_i$. In the following, we establish a bound on the output fidelity of the distillation protocol under a local i.i.d. depolarizing noise model.

Theorem 3. *Consider a Hamiltonian distillation protocol for n EPR pairs $|\Phi^+\rangle_{AB}^{\otimes n}$, each subjected to i.i.d. local depolarizing noise of strength p on Alice's side. Let a Hamiltonian distillation protocol be applied with the following choices: the Hamiltonian used in the twirling step is of the form $H = CDC^\dagger$, where C is drawn from the Clifford group and D is diagonal. The error-detection step is implemented via a projective measurement defined by the orthogonal projectors $\left\{ C \left(\prod_{j=1}^m \frac{I + (-1)^{s_j} X_j}{2} \right) \otimes I^{\otimes (n-m)} C^\dagger : \vec{s} \in \{0, 1\}^m \right\}$. The output fidelity could be lower bounded by:*

$$f_{\text{out}} \geq \frac{1}{1 + (\Delta + 2^{-m}(1 - \Delta - (1 - 3p/4)^n))/(1 - 3p/4)^n}. \quad (9)$$

Here Δ is defined for an arbitrary integer parameter $d \leq n$, given by:

$$\Delta = 2^{-n \left(1 - H(d/n) - d/n \log_2 3 - \delta \right)} + 2^{-n \left(\log_2 \frac{2}{4-3p} + d/n \log_2 \frac{4-3p}{p} \right)}. \quad (10)$$

where $H(\cdot)$ denotes the binary entropy function, and $\delta > 0$ is an arbitrarily small constant.

Although Theorem 3 assumes a joint Clifford measurement, we expect comparable performance when the error-detection step is implemented using local measurements. Our intuition rests on partitioning Pauli errors into an undetectable set $\mathsf{P}_{ud} = C\{I, Z\}^{\otimes n} C^\dagger \setminus \{I\}$ and a detectable set of errors, $\mathsf{P} \setminus \mathsf{P}_{ud}$. While Pauli operators in P_{ud} cannot be scrambled and thus harder to detect, we have established in the proof for Theorem 3 that the occurrence probability of these errors is also very small and can be bounded. For the detectable set $\mathsf{P} \setminus \mathsf{P}_{ud}$, the initial error probabilities are concentrated on low-weight Paulis. However, the twirling effectively uniformizing the probability distribution across the cosets $CX\{I, Z\}^{\otimes n} C^\dagger$ (where $X \in \{I, Z\}^{\otimes n} \setminus \{I\}$). This process smears the probability mass from low-weight Paulis to operators of weight $O(n)$, which ensures high detectability even with local measurements. Analogous to Theorem 2, by measuring $m = O(n)$ qubits, the output fidelity can be made exponentially close to 1 as long as the local depolarizing noise strength p remains below a certain threshold.

IV. NOISE TOLERANCE

In the theory of entanglement distillation, an important performance metric is noise tolerance, defined as the highest physical error rate under which a protocol can asymptotically produce a nonzero rate of EPR pairs with fidelity arbitrarily close to 1. This metric characterizes the robustness of a protocol against severe noise. Noise tolerance is of practical interest for applications such as quantum key distribution, where ultra-long-distance transmission inevitably leads to high error rates that must be suppressed. In QKD, the achievable key rate after classical post-processing is directly determined by the number of high-fidelity EPR pairs that can be distilled. As a result, the noise tolerance of a distillation protocol is closely related to the maximum distance over which a QKD link can yield a nonzero key rate. Below we study the noise tolerance and key rate of a QKD protocol that employs Hamiltonian entanglement distillation as a pre-processing step.

Theorem 4. *Consider an entanglement-based QKD protocol between Alice and Bob. Assume that the shared EPR pairs are subjected to local i.i.d. depolarizing noise of strength p on Bob's side. Alice and Bob group the noisy pairs into blocks of size n and perform Hamiltonian twirling using a diagonal Hamiltonian. They then measure m qubit pairs*

in the Hadamard basis for error detection. The surviving qubit of error detection are measured in the computational basis to generate key bits, followed by standard privacy amplification. The resulting secret key rate is given by:

$$R = \left(\left(1 - \frac{3}{4}p\right)^m \left(1 - \frac{p}{2}\right)^{n-m} + 2^{-m} \left(1 - \left(1 - \frac{p}{2}\right)^n\right) \right) (1 - H(e_p))(1 - m/n), \quad (11)$$

where $H(\cdot)$ denotes the Shannon entropy and $e_p = \frac{2^{-(m+1)}(1 - (1 - \frac{p}{2})^n) + \frac{p}{4-2p}(1 - \frac{3}{4}p)^m(1 - \frac{p}{2})^{n-m}}{2^{-m}(1 - (1 - \frac{p}{2})^n) + (1 - \frac{3}{4}p)^m(1 - \frac{p}{2})^{n-m}}$ is the effective phase error rate inferred from the error-detection step. This protocol tolerates local depolarizing noise up to a threshold p_{tol} , where $p_{\text{tol}} \in [0, 2/3]$ is the solution to

$$\left(1 - \frac{p}{2}\right)^{1-\frac{m}{n}} \left(2 - \frac{3p}{2}\right)^{\frac{m}{n}} = 1. \quad (12)$$

The threshold is obtained when the bit error could be exponentially suppressed. The noise tolerance depends on the number of qubits measured during the error-detection step. The strongest noise tolerance should be achieved when $n - 1$ qubits are measured and only a single EPR pair is retained in each group. These discussions lead us to the following result:

Corollary 1. *The diagonal Hamiltonian error detection plus classical error correction scheme could achieve 33.3% noise tolerance for i.i.d local depolarizing noise model.*

Since an EPR pair subjected to local depolarizing noise with strength $p = 2/3$, or equivalently, error rate of approximately 33.3%, becomes separable, this result reaches the theoretical upper bound. Meaning that we could distill perfect EPR pairs as long as the initial local depolarized noisy states pertain nontrivial entanglement.

V. SIMULATION

In the previous sections, we established theoretical results for general Hamiltonians, demonstrating their efficacy in constructing entanglement distillation protocols. However, real-world Hamiltonians are typically constrained to specific families. To bridge the gap between theory and practice, we present numerical simulations using representative device-native Hamiltonians to demonstrate that our protocol maintains high performance under these experimentally relevant models and requires only experimentally feasible evolution times. We also discuss the impact of skipping Pauli twirling in the presence of non-Pauli noise channels. Finally, we provide additional numerical results on noise tolerance and representative applications including quantum key distribution and quantum repeaters.

A. Performance of Device-native Hamiltonian

The Hamiltonian entanglement distillation protocol is broadly applicable to a variety of quantum systems. Here, we illustrate its application using two representative device-native Hamiltonians: those of Rydberg atom systems and trapped ion systems. In a Rydberg system, a qubit is encoded using the ground state $|g\rangle$ and the Rydberg state $|r\rangle$ of a neutral atom. The system Hamiltonian can be written as

$$H_{\text{rydberg}} = \frac{\Omega}{2} \sum_j (e^{i\phi} |g_j\rangle \langle r_j| + h.c.) - \Delta \sum_j \hat{n}_j + \sum_{j < k} V_{jk} \hat{n}_j \hat{n}_k, \quad (13)$$

where $\hat{n} = |r\rangle \langle r|$. Following the parameters reported in [36], we set the driving frequency to $\Omega = 2\pi \times 1$ MHz and the detuning to $\Delta = 2\pi \times 2.5$ MHz. The interaction strength is given by $V_{jk} = C/|x_j - x_k|^6$, with $C = 2\pi \times 862890$ MHz $\cdot \mu\text{s}^6$. For simplicity, we assume the atoms are arranged in a linear chain with uniform spacing of 6 μm , slightly below the blockade radius, so that the interaction strength could be stronger.

For trapped-ion systems, effective spin-spin interactions can be engineered to realize long-range interaction Hamiltonians of the form [30]

$$H_{\text{ion}} = \sum_{i < j} J_{ij} \hat{\sigma}_i^x \hat{\sigma}_j^x + B \sum_i \hat{\sigma}_i^z. \quad (14)$$

where the couplings are well approximated by a power-law decay $J_{ij} = J_0/|i - j|^\alpha$, with tunable exponent α typically ranging from 0 to 3. We assume the ions are arranged in a uniform linear chain and take the nearest-neighbor coupling strength to be $J_0 = 2\pi \times 1$ kHz. The transverse field is set to $B = 2J_0$, and throughout our simulations we fix $\alpha = 1$,

corresponding to long-range interactions. In addition, we include two idealized Hamiltonians for comparison. The first is the transverse-field Ising model with periodic boundary conditions, given by:

$$\tilde{H}_{TFIM} = J_0 \sum_i \hat{\sigma}_i^x \hat{\sigma}_{i+1}^x + B \sum_i \hat{\sigma}_i^z. \quad (15)$$

with the same parameters J_0 and B as in the trapped-ion case. This is a simplified model of trapped-ion Hamiltonian. The second is a diagonal Hamiltonian $H_{\text{diag}} = \text{diag}(\lambda_1, \dots, \lambda_d)$ satisfying the non-degenerate eigenvalue and gap conditions. Owing to the absence of off-diagonal terms, this Hamiltonian exhibits minimal scrambling and therefore represents the weakest case for error detection in our protocol.

For our simulations, unless stated otherwise, we consider Hamiltonians acting on $n = 5$ qubit pairs, with error detection performed by measuring $m = 3$ pairs in the Hadamard basis, which yields nontrivial performance for diagonal Hamiltonians. We assume a noise model of local i.i.d. depolarizing noise at $p = 0.2$. The performance of different Hamiltonians are compared through yield and fidelity. We adopt the average per-pair fidelity $\bar{f} = f_{\text{out}}^{1/(n-m)}$ as fidelity metric. This normalization enables consistent comparisons between protocols producing varying numbers of entangled pairs.

We begin by demonstrating the asymptotic time performance of the protocol under four distinct Hamiltonian settings. Figure 1 shows the asymptotic fidelity and yield for diagonal, Ising, trapped-ion and Rydberg Hamiltonians as a function of the number of measured qubits. To show the scaling, we simulate Hamiltonians with 10 qubits. We assume that one party of each EPR pair is subject to local depolarizing noise of strength $p = 0.2$, therefore the initial average fidelity of $\bar{f}_0 = 1 - 3p/4 = 0.85$ before distillation. Ideally, increasing the number of measured qubits is expected to improve fidelity at the cost of a reduced yield. Overall, the trends observed in Fig. 1 are consistent with these expectations. The trapped-ion Hamiltonian and its periodic-boundary Ising approximation exhibit comparable performance. Although omitting the long-range interactions in the Ising model reduces its scrambling strength, the periodic boundary condition enhances qubit connectivity, partially compensating for this effect and resulting in similar distillation performance. The Rydberg Hamiltonian achieves smaller fidelity improvements compared to the trapped-ion case. This can be attributed to the faster spatial decay of interactions in Rydberg systems, which scale as r^{-6} , whereas the trapped-ion model considered here assumes $\alpha = 1$, corresponding to a slower r^{-1} decay and hence stronger long-range coupling. As a result, the trapped-ion Hamiltonian provides more effective error scrambling. The diagonal Hamiltonian yields the poorest performance among all Hamiltonians, due to its inability to detect and suppress Z -type. Compared with a single round of the recurrence method, the Hamiltonian-based protocol achieves substantially higher fidelity at the cost of reduced yield. This trend would also persist when both methods are applied over multiple rounds. Importantly, in realistic experimental settings, implementing multiple distillation rounds leads to great overhead due to the need for measurement feedback and the requirement to physically regroup qubits that may be spatially separated. Therefore, the ability of the Hamiltonian-based method to achieve higher fidelity within fewer rounds constitutes a significant practical advantage.

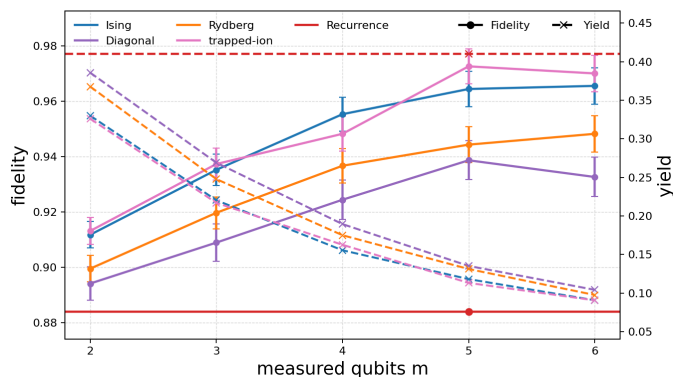


FIG. 1. Distillation performance as a function of the number of measurement qubits. The solid line with circle markers denotes the output fidelity, while the dashed line with cross markers denotes the yield. We consider a ten-qubit Hamiltonian with local depolarizing noise of strength $p = 0.2$.

In Fig. 2, we examine the distillation performance under varying strengths of local depolarizing noise. The results show that the periodic-boundary Ising model achieves performance comparable to that of the trapped-ion Hamiltonian. Moreover, the trapped-ion Hamiltonian consistently outperforms the Rydberg Hamiltonian, which in turn outperforms the diagonal Hamiltonian across the entire noise range. Comparing this figure at point $p = 0.2$ and the previous figure demonstrates that enlarging the Hamiltonian system and measuring more qubits substantially enhances distillation

performance. From the above asymptotic analysis, we conclude that realistic Hamiltonians consistently outperform diagonal Hamiltonians across different measurement and noise settings. This observation implies that analytical results derived for diagonal Hamiltonians can be interpreted as conservative lower bounds for the performance of many practically relevant Hamiltonians, for which closed-form expressions are often difficult to obtain. Accordingly, in the following simulation sections, we focus on the more practically relevant trapped-ion and Rydberg Hamiltonians.

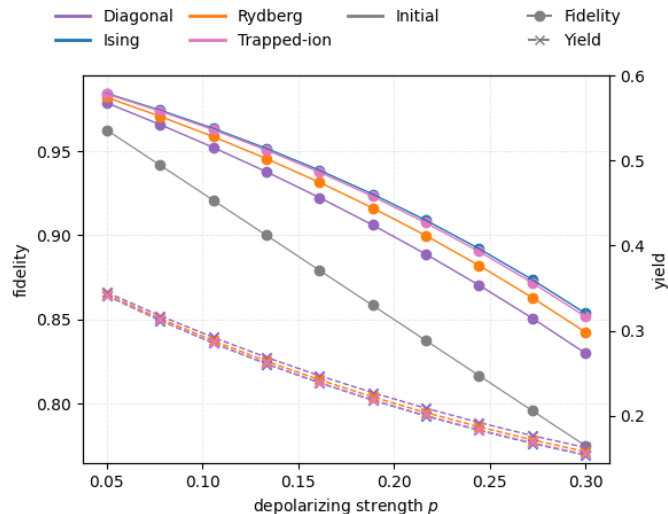


FIG. 2. Distillation performance as a function of the depolarizing noise strength. The solid line with circle markers denotes the output fidelity, while the dashed line with cross markers denotes the yield. We consider a six-qubit Hamiltonian with three measurement qubits.

We now consider the finite-time effects of different Hamiltonians, which are crucial for realistic applications, as current quantum platforms have limited coherence times. The Rydberg platform operates at frequencies on the order of MHz, while trapped-ion systems are typically in the kHz range. To enable a meaningful comparison, we define a unit of time as $1/2\pi \mu\text{s}$ for Rydberg atoms and $1/2\pi \text{ms}$ for trapped ions, allowing both time scales to be displayed on the same plot in Figure 3. The asymptotic performance for both Hamiltonians can be approximated in Figure 2, where the trapped-ion Hamiltonian has fidelity of approximately 0.925 and the Rydberg Hamiltonian reaches 0.91.

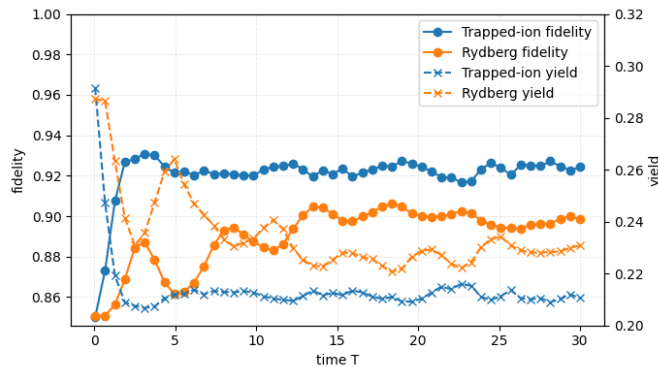


FIG. 3. Finite-time distillation performance for trapped-ion and Rydberg Hamiltonians. The characteristic evolution times are at the microsecond (μs) scale for the Rydberg Hamiltonian and at the millisecond (ms) scale for the trapped-ion Hamiltonian. The solid line with circle markers denotes the output fidelity, while the dashed line with cross markers denotes the yield.

Figure 3 shows that evolving the trapped-ion Hamiltonian for just 2 units of time (about $1/\pi \text{ms}$) is sufficient to achieve fidelity higher than asymptotic performance. For reference, experiments in [37] demonstrate coherence times of roughly 2 ms over hundreds of qubits, indicating that Hamiltonian entanglement distillation is already practical on current devices. For the Rydberg Hamiltonian, fidelity reaches a plateau close to its asymptotic fidelity at about 13 unit time (about $2\mu\text{s}$) and then becomes quite stable in this high fidelity plateau. This again reflects the weaker

scrambling power of the Rydberg Hamiltonian compared to trapped-ion Hamiltonian, requiring longer evolution times to approach its asymptotic fidelity. Both Hamiltonians exhibit oscillatory behavior in fidelity, with the effect being more significant for the Rydberg Hamiltonian. This behavior can be attributed to the presence of quasi-degenerate eigenvalue gaps, or equivalently, very small differences in the eigenvalue gaps, which compromise efficient scrambling over time. Importantly, these results indicate that the Hamiltonian-based protocol remains effective in the presence of moderate spectral degeneracies and does not require a fully nondegenerate spectrum.

B. Non-Pauli Noises

In our protocol in Sec II, we include a step of Pauli twirling to convert arbitrary noise into Pauli noise. While this is a digital operation, it can still be implemented on many analog simulators. To support our claim that the protocol performs well even without this step, we analyze the effect of Pauli twirling on non-Pauli noise, demonstrating that a purely analog implementation remains effective. Specifically, we focus on amplitude damping noise, which is commonly encountered in trapped-ion and neutral-atom systems. This noise is both non-Pauli and non-unital, making it challenging to treat in many theoretical settings. In our simulations, we consider a local depolarizing noise with strength $p = 0.2$, followed by a local amplitude damping noise with varying strength γ . This allows us to investigate how the protocol performs in a realistic analog scenario without relying on Pauli twirling.

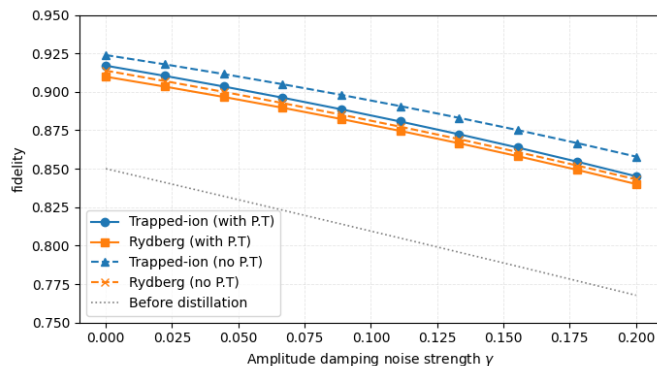


FIG. 4. Distillation performance with and without Pauli twirling. The solid line with circle markers corresponds to the case with Pauli twirling, while the dashed line with triangle markers corresponds to the case without twirling.

The performance of different Hamiltonians, both with and without Pauli twirling, is shown in Figure 4. From Figure 4, we observe that for local amplitude damping noise, when measured in the hadamard basis, the protocol without Pauli twirling actually achieves higher fidelity performance than the Pauli twirling version. This is potentially because the Pauli Liouville representation of amplitude damping channel is

$$\mathcal{R}_{\text{AD}} = \begin{pmatrix} 1 & 0 & 0 & 0 \\ 0 & \sqrt{1-\gamma} & 0 & 0 \\ 0 & 0 & \sqrt{1-\gamma} & 0 \\ \gamma & 0 & 0 & 1-\gamma \end{pmatrix}, \quad (16)$$

in the Pauli basis $2\{I, \sigma_x, \sigma_y, \sigma_z\}$ where additional Z operators are introduced before Pauli twirling and thus being more probably to be detected through the X-basis measurement. Therefore even in the absence of Pauli twirling, the protocol remains effective, demonstrating its robustness for purely analog implementations.

C. Noise Tolerance

Finally, we present additional numerical results on noise tolerance. Figure 5(a) shows the noise tolerance for different fractions of measured qubits in the asymptotic qubits number n limit. The blue region below the curve are the tolerable error region while gray region above would result in the protocol to output zero EPR pair. Measuring all but one qubit is represented as the rightmost point of the curve, which allows the protocol to approach the $1/3$ threshold, while measuring only half of the qubits reduces the tolerable error rate to $(5 - \sqrt{13})/6 \approx 23\%$. The noise tolerance for finite n and m are shown in Figure 5(b). For a Hamiltonian of size $n = 20$, the maximum tolerable

error rate is approximately 26%. When the qubit number increases to $n = 50$, the noise tolerance exceeds 30%. Note that when the measuring qubits is very few, the noise tolerance is quite low, even less than the noise tolerance for one-way hashing protocol. This is because in the diagonal Hamiltonian twirling step, we would introduce more phase error for the states that already have X -error. So if the probability of those components are not well suppressed, we are introducing too much phase error and compromise the further one-way distillation step. To guarantee good noise tolerance and practical performance, we typically need to measure $O(n)$ qubits for error detection.

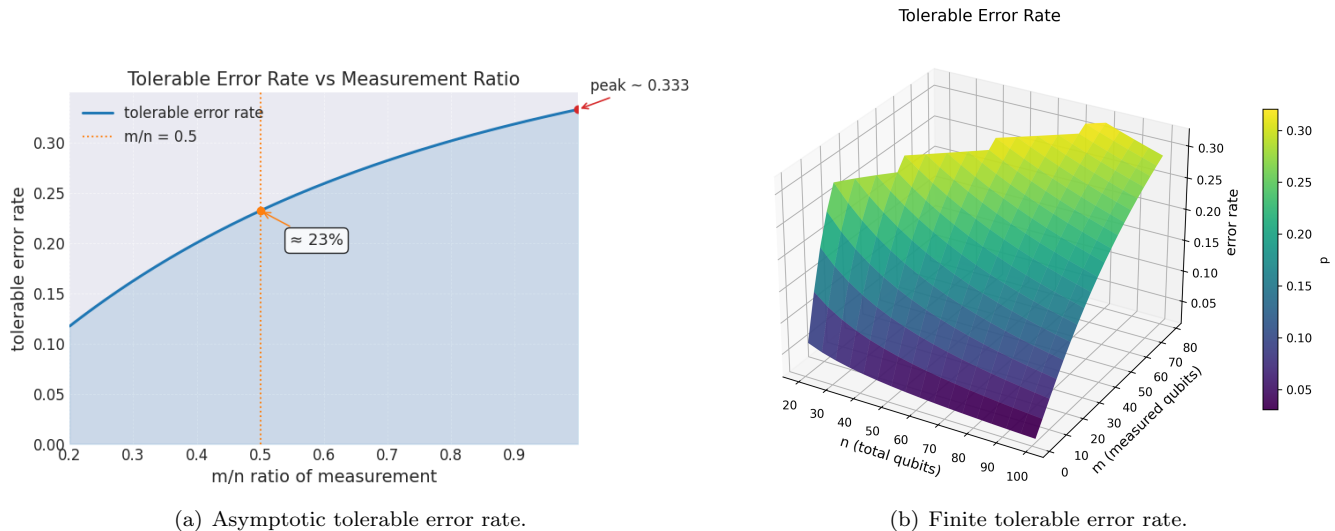


FIG. 5. Tolerable error rates under varying conditions: (a) asymptotic behavior as a function of the measurement qubit ratio m/n ; (b) performance for finite system sizes where $n, m \leq 100$.

To illustrate the practical implications of noise tolerance in quantum networks, we consider two representative applications. The first is the maximum achievable transmission distance in quantum key distribution. The second concerns quantum repeater networks: specifically, the largest separation between neighboring repeaters for which the distilled entanglement can still exceed a certain fidelity threshold. Following recent work on quantum repeaters [38], we set the fidelity threshold to 90%, which could lead to the violation of the Bell inequality up to approximately 2.5. Further details on the channel noise model and simulation parameters are provided in the Appendix C and references [38, 39]. Figure 6(a) compares the maximum transmission distance of different QKD protocols versus the photon bit error rate e_d determined by the quantum channel. The Hamiltonian-based protocol considered here is introduced in Theorem 4. Specifically, we use a protocol based on a 15-qubit diagonal Hamiltonian, with error detection performed on 12 qubits. The Hamiltonian-based protocol attains a substantially larger maximum distance, outperforming the recurrence protocol even after two rounds of iteration. This improvement reflects the enhanced noise tolerance enabled by Hamiltonian-based distillation. Figure 6(b) shows the distilled fidelity versus transmission distance. Since no error correction could be applied in this case, we assume Hamiltonian in Theorem 2 instead of diagonal Hamiltonian in this setting. Note that when no distillation is performed, the fidelity drops below 90% at about 120km, while two-way method can boost this 90% fidelity threshold to about 300km, with Hamiltonian-based method achieving highest separation distance.

VI. OUTLOOK

In this work, we introduced a class of entanglement distillation protocols based on Hamiltonian evolution. In contrast to conventional digital schemes, our approach exploits the intrinsic scrambling dynamics of many-body Hamiltonians to enable efficient error detection and high-performance distillation. We established a quantitative connection between a Hamiltonian's scrambling capability and its distillation performance, showing that generic interacting Hamiltonians provide sufficient scrambling for this task. We further discuss the problem of noise tolerance and show strong performance in this metric of the Hamiltonian based protocol.

On the practical side, we validated our protocol through numerical simulations of experimentally relevant platforms, including Rydberg atom arrays and trapped-ion systems. The results demonstrate favorable distillation performance achievable within short, experimentally accessible evolution times. Additional numerical results on representative

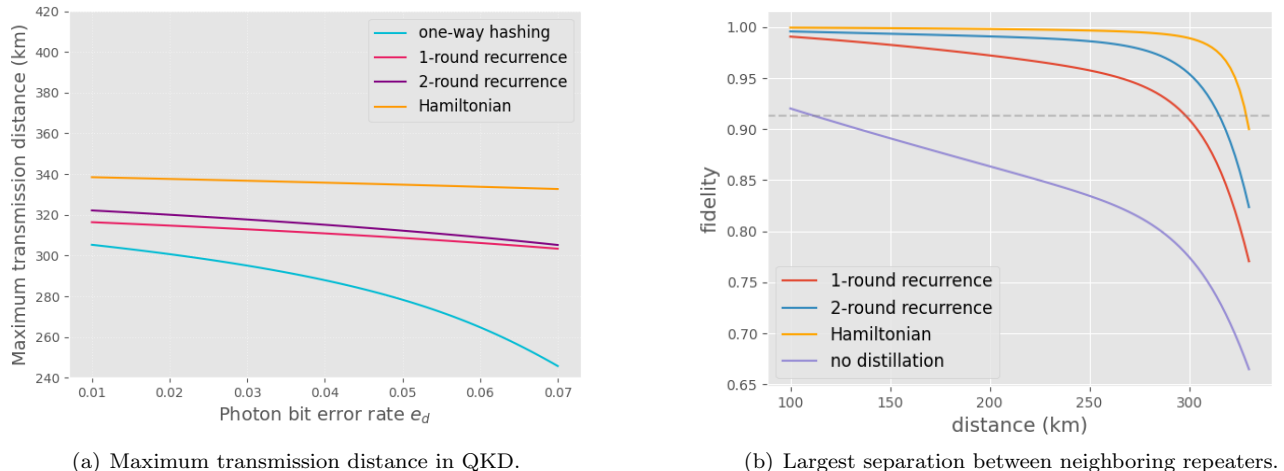


FIG. 6. Noise tolerance shown in practical application.

applications in quantum key distribution and quantum repeaters show that our protocol gives sufficient high noise tolerance that could enable longer maximum transmission distance than conventional methods like recurrence protocol with few rounds. Our protocol requires only evolution under a native Hamiltonian followed by local measurements, avoiding the need for fine-grained pulse-level control, complex circuit compilation, or high-overhead quantum error correction. This makes it well suited for near-term implementation on existing analog quantum simulators.

Several directions for future work naturally arise. A central theoretical question is to quantify the time complexity required to reach a target fidelity, which is closely tied to the growth of out-of-time-order correlators and the rate of information scrambling. Establishing explicit bounds between scrambling rates and distillation time would provide deeper insight into the power of analog dynamics for quantum information processing. In addition, it would be interesting to extend this framework to broader classes of dynamics, including driven or Floquet systems, and to identify Hamiltonians with enhanced scrambling properties. Optimizing the underlying interactions or driving protocols may further reduce the required evolution time, enabling even more efficient entanglement distillation on near-term hardware. Finally, since quantum networks are designed based on optical system, whether this protocol could be generalized to continuous-variable system is also an interesting question for future efforts.

ACKNOWLEDGMENTS

We thank Michael Gullans, Shiv Akshar Yadavalli, Chushi Qin, Xiaodi Wu, Yingkang Cao, Haohai Shi, Connor Clayton, Mattias Ehatamm, Hongzheng Zhu, Kecheng Liu, Zhenyu Du, Shengfan Liu for their helpful discussions. Z.X acknowledges funding and support from Joint Center for Quantum Information and Computer Science (QuICS) Lancelos Graduate Fellowship. G.L. acknowledges the National Natural Science Foundation of China Grant No. 12575023.

-
- [1] C. H. Bennett and G. Brassard, “Quantum cryptography: Public key distribution and coin tossing,” in *Proceedings of IEEE International Conference on Computers, Systems and Signal Processing*, (Bangalore, India), pp. 175–179, IEEE, 1984. Reprinted in *Theoretical Computer Science* 560, 7–11 (2014).
 - [2] C. H. Bennett, G. Brassard, C. Crépeau, R. Jozsa, A. Peres, and W. K. Wootters, “Teleporting an unknown quantum state via dual classical and einstein-podolsky-rosen channels,” *Physical Review Letters*, vol. 70, no. 13, pp. 1895–1899, 1993.
 - [3] J. I. Cirac, A. K. Ekert, S. F. Huelga, and C. Macchiavello, “Distributed quantum computation over noisy channels,” *Physical Review A*, vol. 59, no. 6, pp. 4249–4254, 1999.
 - [4] D. Gottesman and I. L. Chuang, “Demonstrating the viability of universal quantum computation using teleportation and single-qubit operations,” *Nature*, vol. 402, no. 6760, pp. 390–393, 1999.
 - [5] R. Van Meter and S. J. Devitt, “The path to scalable distributed quantum computing,” *Computer*, vol. 49, no. 9, pp. 31–42, 2016.

- [6] D. Gottesman, T. Jennewein, and S. Croke, “Longer-baseline telescopes using quantum repeaters,” *Phys. Rev. Lett.*, vol. 109, p. 070503, Aug 2012.
- [7] C. H. Bennett, D. P. DiVincenzo, J. A. Smolin, and W. K. Wootters, “Mixed-state entanglement and quantum error correction,” *Physical Review A*, vol. 54, no. 5, pp. 3824–3851, 1996.
- [8] D. Gottesman and H.-K. Lo, “Proof of security of quantum key distribution with two-way classical communications,” *IEEE Transactions on Information Theory*, vol. 49, no. 2, pp. 457–475, 2003.
- [9] I. Devetak and A. Winter, “Distillation of secret key and entanglement from quantum states,” *Proceedings of the Royal Society A: Mathematical, Physical and Engineering Sciences*, vol. 461, no. 2053, pp. 207–235, 2005.
- [10] H.-F. Chau, “Practical scheme to share a secret key through a quantum channel with a 27.6% bit error rate,” *Physical Review A*, vol. 66, no. 6, p. 060302, 2002.
- [11] B. Kraus, N. Gisin, and R. Renner, “Lower and upper bounds on the secret-key rate for quantum key distribution protocols using one-way classical communication,” *Physical Review Letters*, vol. 95, no. 8, p. 080501, 2005.
- [12] S. Watanabe, R. Matsumoto, T. Uyematsu, and Y. Kawano, “Key rate of quantum key distribution with hashed two-way classical communication,” *Physical Review A*, vol. 76, no. 3, p. 032312, 2007.
- [13] Z. Du, G. Liu, X. Zhang, and X. Ma, “Advantage distillation for quantum key distribution,” *Quantum Science and Technology*, vol. 10, p. 015050, dec 2024.
- [14] A. Gu, L. Leone, K. Goodenough, and S. Khatri, “Constant overhead entanglement distillation via scrambling,” 2025.
- [15] J.-W. Pan, C. Simon, Āaslav Brukner, and A. Zeilinger, “Entanglement purification for quantum communication,” *Nature*, vol. 410, no. 6832, pp. 1067–1070, 2001.
- [16] N. Kalb, A. A. Reiserer, P. C. Humphreys, J. J. W. Bakermans, S. J. Kamberling, N. H. Nickerson, S. C. Benjamin, D. J. Twitchen, M. Markham, and R. Hanson, “Entanglement distillation between solid-state quantum network nodes,” *Science*, vol. 356, no. 6341, pp. 928–932, 2017.
- [17] V. Krutyanskiy, M. Canteri, M. Meraner, J. Bate, V. Krcmarsky, J. Schupp, N. Sangouard, and B. P. Lanyon, “Telecom-wavelength quantum repeater node based on a trapped-ion processor,” *Phys. Rev. Lett.*, vol. 130, p. 213601, May 2023.
- [18] C. Liu, T. Tu, P.-Y. Li, X. Liu, X.-Y. Zhu, Z.-Q. Zhou, C.-F. Li, and G.-C. Guo, “Towards entanglement distillation between atomic ensembles using high-fidelity spin operations,” *Communications Physics*, vol. 5, no. 1, p. 67, 2022.
- [19] S. Ecker, P. Sohr, L. Bulla, M. Huber, M. Bohmann, and R. Ursin, “Experimental single-copy entanglement distillation,” *Phys. Rev. Lett.*, vol. 127, p. 040506, Jul 2021.
- [20] G. Q. AI and Collaborators, “Quantum error correction below the surface code threshold,” *Nature*, vol. 638, no. 8052, pp. 920–926, 2025.
- [21] Y. Peng, J. Young, P. Liu, and X. Wu, “Simuq: A framework for programming quantum hamiltonian simulation with analog compilation,” *Proc. ACM Program. Lang.*, vol. 8, Jan. 2024.
- [22] I. Bloch, J. Dalibard, and S. Nascimbène, “Quantum simulations with ultracold quantum gases,” *Nature Physics*, vol. 8, no. 4, pp. 267–276, 2012.
- [23] M.-G. Hu, Y. Liu, D. D. Grimes, Y.-W. Lin, A. H. Gheorghie, R. Vexiau, N. Bouloufa-Maafa, O. Dulieu, T. Rosenband, and K.-K. Ni, “Direct observation of bimolecular reactions of ultracold krb molecules,” *Science*, vol. 366, no. 6469, pp. 1111–1115, 2019.
- [24] H. Bernien, S. Schwartz, A. Keesling, H. Levine, A. Omran, H. Pichler, S. Choi, A. S. Zibrov, M. Endres, M. Greiner, V. Vuletić, and M. D. Lukin, “Probing many-body dynamics on a 51-atom quantum simulator,” *Nature*, vol. 551, no. 7682, pp. 579–584, 2017.
- [25] M. C. Tran, D. K. Mark, W. W. Ho, and S. Choi, “Measuring arbitrary physical properties in analog quantum simulation,” *Phys. Rev. X*, vol. 13, p. 011049, Mar 2023.
- [26] Z. Liu, Z. Hao, and H.-Y. Hu, “Predicting arbitrary state properties from single hamiltonian quench dynamics,” *Phys. Rev. Res.*, vol. 6, p. 043118, Nov 2024.
- [27] R. Renner, N. Gisin, and B. Kraus, “Information-theoretic security proof for quantum-key-distribution protocols,” *Phys. Rev. A*, vol. 72, p. 012332, Jul 2005.
- [28] M. Gärttner, J. G. Bohnet, A. Safavi-Naini, M. L. Wall, J. J. Bollinger, and A. M. Rey, “Measuring out-of-time-order correlations and multiple quantum spectra in a trapped-ion quantum magnet,” *Nature Physics*, vol. 13, no. 8, pp. 781–786, 2017.
- [29] P. Richerme, Z.-X. Gong, A. Lee, C. Senko, J. Smith, M. Foss-Feig, S. Michalakis, A. V. Gorshkov, and C. Monroe, “Non-local propagation of correlations in quantum systems with long-range interactions,” *Nature*, vol. 511, no. 7508, pp. 198–201, 2014.
- [30] C. Monroe, W. C. Campbell, L.-M. Duan, Z.-X. Gong, A. V. Gorshkov, P. W. Hess, R. Islam, K. Kim, N. M. Linke, G. Pagano, P. Richerme, C. Senko, and N. Y. Yao, “Programmable quantum simulations of spin systems with trapped ions,” *Rev. Mod. Phys.*, vol. 93, p. 025001, Apr 2021.
- [31] S. Massar and S. Popescu, “Optimal extraction of information from finite quantum ensembles,” *Phys. Rev. Lett.*, vol. 74, pp. 1259–1263, Feb 1995.
- [32] X. song Ma, S. Kropatschek, W. Naylor, T. Scheidl, J. Kofler, T. Herbst, A. Zeilinger, and R. Ursin, “Experimental quantum teleportation over a high-loss free-space channel,” *Opt. Express*, vol. 20, pp. 23126–23137, Oct 2012.
- [33] R. Horodecki, P. Horodecki, M. Horodecki, and K. Horodecki, “Quantum entanglement,” *Rev. Mod. Phys.*, vol. 81, pp. 865–942, Jun 2009.
- [34] S. Wehner, D. Elkouss, and R. Hanson, “Quantum internet: A vision for the road ahead,” *Science*, vol. 362, no. 6412, p. eaam9288, 2018.

- [35] W. K. Wootters and B. D. Fields, “Optimal state-determination by mutually unbiased measurements,” *Annals of Physics*, vol. 191, no. 2, pp. 363–381, 1989.
- [36] QuEra Computing Inc. and Bloqade.jl Developers, “Bloqade.jl documentation: Hamiltonians.” <https://queracomputing.github.io/Bloqade.jl/dev/hamiltonians/>, 2024. Accessed: 2026-01-12.
- [37] S.-A. Guo, Y.-K. Wu, J. Ye, L. Zhang, W.-Q. Lian, R. Yao, Y. Wang, R.-Y. Yan, Y.-J. Yi, Y.-L. Xu, B.-W. Li, Y.-H. Hou, Y.-Z. Xu, W.-X. Guo, C. Zhang, *et al.*, “A site-resolved two-dimensional quantum simulator with hundreds of trapped ions,” *Nature*, vol. 630, pp. 613–618, June 2024.
- [38] W.-Z. Liu, Y.-B. Zhou, J.-P. Chen, B. Wang, A. Teng, X.-W. Han, G.-C. Liu, Z.-J. Zhang, Y. Yang, F.-G. Liu, C.-H. Xue, B.-W. Yang, J. Yang, C. Zeng, D.-R. Pan, M.-Y. Zheng, X. Zhang, S. Cao, Y.-Z. Zhen, Y. Xiao, H. Li, L. You, X. Ma, Q. Zhao, F. Xu, Y. Wang, Y. Wan, Q. Zhang, and J.-W. Pan, “Long-lived remote ion-ion entanglement for scalable quantum repeaters,” *Nature*, feb 2026.
- [39] Z. Xu, Y. Huang, and X. Ma, “Enhanced analysis for the decoy-state method,” *Advanced Quantum Technologies*, vol. n/a, no. n/a, p. 2400687.
- [40] A. A. Mele, “Introduction to Haar Measure Tools in Quantum Information: A Beginner’s Tutorial,” *Quantum*, vol. 8, p. 1340, May 2024.
- [41] Z. Webb, “The clifford group forms a unitary 3-design,” *Quantum Info. Comput.*, vol. 16, p. 1379–1400, Nov. 2016.
- [42] H. Zhu, “Multiqubit clifford groups are unitary 3-designs,” *Physical Review A*, vol. 96, Dec. 2017.
- [43] B. Collins and P. Śniady, “Integration with respect to the haar measure on unitary, orthogonal and symplectic groups,” *Communications in Mathematical Physics*, vol. 264, no. 3, pp. 773–795, 2006.
- [44] X. Ma, P. Zeng, and H. Zhou, “Phase-matching quantum key distribution,” *Phys. Rev. X*, vol. 8, p. 031043, Aug 2018.
- [45] H.-T. Zhu, Y. Huang, W.-X. Pan, C.-W. Zhou, J. Tang, H. He, M. Cheng, X. Jin, M. Zou, S. Tang, X. Ma, T.-Y. Chen, and J.-W. Pan, “Field test of mode-pairing quantum key distribution,” *Optica*, vol. 11, pp. 883–888, Jun 2024.
- [46] C.-Y. Lu and J.-W. Pan, “Quantum-dot single-photon sources for the quantum internet,” 2023.

Appendix A: Preliminary

1. Basic notations and quantities

Let us start from the basic notations of this work. We denote the Hilbert space as \mathcal{H} . A quantum state ρ is a Hermitian operator in the Hilbert space which has unity trace. When this state is a pure state, sometimes we will write it as a vector $|\psi\rangle$, which in terms meaning that the density matrix is $|\psi\rangle\langle\psi|$. The physical operation $\mathcal{N} : \mathcal{H} \rightarrow \mathcal{H}$ that maps a quantum state to another quantum state is called a quantum channel, which should satisfy CPTP condition. Here CP means completely positive, that is for any positive operator $\sigma \in \mathcal{H} \otimes \mathcal{H}_0$, the channel should have $\mathcal{N} \otimes \mathcal{I}(\sigma) > 0$ with \mathcal{I} being the identity channel in Hilbert space \mathcal{H}_0 . The measurement of a quantum state is performed by a positive operator valued measurement, or POVM $\{M_0, \dots, M_k\}$ such that each $M_i \in \mathcal{H}$ is a positive operator and $\sum_i M_i = I$.

In this paper, certain quantum states, channels, and measurements will be frequently used. The most important states are the four Bell state on a bipartite system $\mathcal{H}_A \otimes \mathcal{H}_B$:

$$\begin{aligned} |\Phi^+\rangle &= \frac{1}{\sqrt{2}} (|00\rangle + |11\rangle), \\ |\Phi^-\rangle &= \frac{1}{\sqrt{2}} (|00\rangle - |11\rangle), \\ |\Psi^+\rangle &= \frac{1}{\sqrt{2}} (|01\rangle + |10\rangle), \\ |\Psi^-\rangle &= \frac{1}{\sqrt{2}} (|01\rangle - |10\rangle). \end{aligned} \tag{A1}$$

Among the four states, $|\Phi^+\rangle$, sometimes called EPR state, is of particular interest due to its symmetry. For example, it can be extended naturally into the $2n$ -qubit EPR state

$$|\Phi^+\rangle^{\otimes n} = \sum_{i=0}^{2^n-1} |ii\rangle, \tag{A2}$$

where the first $|i\rangle$ indicates the state in system \mathcal{H}_A and the second $|i\rangle$ indicate the state in system \mathcal{H}_B . One important property of EPR state enabling our work is the following identity:

$$U_A |\Phi^+\rangle_{AB} = U_B^T |\Phi^+\rangle_{AB}. \tag{A3}$$

Together with the fact that $(U^T)^\dagger = U^*$, we can see that $U_A U_B^* |\Phi^+\rangle_{AB} = |\Phi^+\rangle_{AB}$. The EPR state serves as a fundamental resource in quantum information science. However, during the transmission of EPR states, noise is inevitable. Two commonly encountered noise models are depolarizing noise and dephasing noise. The single-qubit depolarizing channel with noise strength p is defined as

$$\mathcal{D}_p(\rho) = (1-p)\rho + p\frac{I}{2}, \tag{A4}$$

Since for arbitrary single qubit state ρ we have $\frac{1}{4}(\rho + X\rho X + Y\rho Y + Z\rho Z) = \frac{I}{2}$. This channel can be also written as

$$\mathcal{D}_p(\rho) = (1 - \frac{3}{4}p)\rho + \frac{p}{4}X\rho X + \frac{p}{4}Y\rho Y + \frac{p}{4}Z\rho Z, \tag{A5}$$

The above two definition are equivalent. This channel isotropically randomizes the state and models symmetric errors in all Pauli directions. Another useful channel is the dephasing channel with error rate p is given by

$$\mathcal{Z}_p(\rho) = (1-p)\rho + pZ\rho Z. \tag{A6}$$

This noise preserves populations in the computational basis while suppressing off-diagonal coherence. In our main theorem, we will consider a special case of the dephasing channel, called global complete dephasing channel, defined by

$$\Delta(\rho) = \mathcal{Z}_{1/2}^{\otimes n}(\rho). \tag{A7}$$

This channel removes all off-diagonal elements of a density matrix in the computational basis, effectively turning it into a classical mixture.

Both depolarizing noise and dephasing noise belong to the class of *Pauli channels*. A Pauli channel is a quantum channel whose action can be expressed as a probabilistic mixture of Pauli operators. For an n -qubit system, a Pauli channel takes the form of

$$\Lambda(\rho) = \sum_{P \in \mathcal{P}_n} c_P P \rho P, \quad (\text{A8})$$

where $\mathcal{P}_n = \{I, X, Y, Z\}^{\otimes n}$ denotes the n -qubit Pauli group (up to phases), and $\{c_P\}$ is a probability distribution. Local depolarizing noise corresponds to the single qubit case in which all non-identity Pauli operators occur with equal probability, while dephasing noise corresponds to Pauli channels supported only on Z -type operators. Pauli channels are diagonal in the Pauli operator basis and naturally arise after Pauli twirling, making them a convenient and widely used noise model in quantum information theory. Suppose there is a Pauli channel Λ_{AB} that acts on Hilbert space $\mathcal{H}_A \otimes \mathcal{H}_B$ with $\mathcal{H}_A, \mathcal{H}_B$ having equal dimension. Then there always exists a Pauli channel Λ_A that acts on \mathcal{H}_A such that $\Lambda_{AB}(|\Phi^+\rangle_{AB}) = (\Lambda_A \otimes \mathcal{I}d)(|\Phi^+\rangle_{AB})$. Here $\mathcal{I}d$ denotes the identity channel. This can be shown by again considering Eq. (A3). For a Pauli operator in space $\mathcal{H}_A \otimes \mathcal{H}_B$, we can decompose it as $P \otimes Q$ where $P \in \mathcal{H}_A, Q \in \mathcal{H}_B$. Then $(P \otimes Q)|\Phi^+\rangle = (PQ^T \otimes I)|\Phi^+\rangle$, which becomes an error operator on system \mathcal{H}_A .

When an ideal EPR pair is subjected to Pauli noise, the system evolves into a Bell-diagonal state. Consider, for instance, the maximally entangled state $|\Phi^+\rangle = \frac{1}{\sqrt{2}}(|00\rangle + |11\rangle)$. If one subsystem undergoes a local depolarizing channel, the global state transforms into the density matrix:

$$\rho = (1-p)|\Phi^+\rangle\langle\Phi^+| + \frac{p}{3}(|\Phi^-\rangle\langle\Phi^-| + |\Psi^+\rangle\langle\Psi^+| + |\Psi^-\rangle\langle\Psi^-|). \quad (\text{A9})$$

This highly symmetric mixed state, representing a uniform mixture of the target Bell state with the orthogonal error states, is also called the Werner state.

For quantum measurement, there is a set of measurement basis of particular interest, which is called the Mutually Unbiased Basis (MUB).

Definition 2 (Mutually unbiased bases). *Let \mathcal{H} be a d -dimensional Hilbert space. Two orthonormal bases*

$$\mathcal{B} = \{|e_i\rangle\}_{i=1}^d, \quad \mathcal{B}' = \{|f_j\rangle\}_{j=1}^d$$

are called mutually unbiased if

$$|\langle e_i | f_j \rangle|^2 = \frac{1}{d} \quad \text{for all } i, j.$$

Suppose in basis \mathcal{B} we prepare a classical mixture of the basis vectors, i.e.

$$\rho_{\mathcal{B}} = \sum_i \lambda_i |e_i\rangle\langle e_i|. \quad (\text{A10})$$

And we perform measurement in \mathcal{B}' basis. The probability of outcome $|f_j\rangle$ occurs is

$$\begin{aligned} p_j &= \langle f_j | \sum_i \lambda_i |e_i\rangle\langle e_i | f_j \rangle \\ &= \frac{1}{d} \sum_i \lambda_i = \frac{1}{d}. \end{aligned} \quad (\text{A11})$$

That is to say, the measurement outcome in a mutually unbiased basis is uniformly random for any classical mixture state in one basis.

The distance of two quantum state is often measured via fidelity, which, for two mixed state ρ and σ , is

$$F(\sigma, \rho) = \left(\text{tr} \sqrt{\sqrt{\sigma} \rho \sqrt{\sigma}} \right)^2. \quad (\text{A12})$$

When σ is a pure state, say $|\psi\rangle$, the above formula could be reduced to $F(|\psi\rangle, \rho) = \langle \psi | \rho | \psi \rangle$. In our paper, we will mainly focus on the case where $|\psi\rangle = |\Phi^+\rangle$, the EPR state. And the goal is to do some operations on state ρ to increase its fidelity with $|\Phi^+\rangle$.

2. Entanglement distillation

More details on entanglement distillation could be found in [7]. Here we just do a brief review of basic one-way and two-way protocols. We first introduce the one-way hashing method which is very standard in quantum key distribution. Through the discussion of one-way method we motivate why two-way detection based methods are desired and then introduce basic two-way protocols.

a. One-way hashing method.

The one-way hashing method is an error-correction based method. Due to its equivalency to classical post-processing in the QKD setting, it has become the standard in QKD. Also since it does not discard qubit probabilistically, its yield is higher than most two-way methods in low noise regions.

The hashing method involves the following steps:

1. **Parameter estimation:** Alice and Bob first choose some noisy states and measure in X or Z basis. After measurement they compare their results to estimate the bit error rate e_b and phase error rate e_p .
2. **Bit error correction:** Following parameter estimation, suppose n entangled pairs remain with a bit error rate e_b . Alice and Bob agree on a binary hashing matrix B^e of dimension $n \times nH(e_b)$, drawn from a universal hashing family. They compute the hashing results into the final $nH(e_b)$ pairs (the "check" qubits) by performing CNOT operations determined by the matrix entries: for every non-zero element $B_{i,j}^e = 1$, a CNOT gate is applied between the i -th data qubit and the corresponding check qubit. Subsequently, both parties measure these check qubits in the Z -basis. Alice transmits her outcome vector \mathbf{s}_A to Bob, who combines it with his local result \mathbf{s}_B to compute the error syndrome $\mathbf{s} = \mathbf{s}_A \oplus \mathbf{s}_B$. Finally, Bob decodes this syndrome to identify the error configuration and applies the necessary bit-flip corrections to the remaining $n - nH(e_b)$ data pairs.
3. **Phase error correction:** Similar to phase error correction, they agree on a hashing matrix B^p of dimension $n(1 - H(e_b)) \times nH(e_p)$ and compute the hashing results into the current last $nH(e_p)$ qubits. This time they perform CNOT in the Hadamard basis and measure the last $nH(e_p)$ qubits in X -basis measurement. Similarly Alice sends her measurement result to Bob. Bob does the decoding and performs phase-flip correction on remaining $n(1 - H(e_b) - H(e_p))$ qubits.

After performing both bit-error correction and phase-error correction, the remaining $n(1 - H(e_b) - H(e_p))$ pairs converge to perfect EPR pairs in the asymptotic limit $n \rightarrow \infty$. The corresponding asymptotic yield of the one-way hashing protocol is therefore

$$Y = 1 - H(e_b) - H(e_p). \quad (\text{A13})$$

When $e_b = e_p \approx 11\%$, this yield vanishes, indicating that one-way entanglement distillation fails beyond this error threshold. Consequently, there exist entangled states that are not distillable by one-way protocols alone. In such cases, it is necessary to first reduce the error rates below this threshold—using, for example, a two-way or pre-processing distillation step—before applying one-way hashing to obtain high-fidelity EPR pairs. In the following we introduce the most basic two-way protocol, the recurrence protocol.

b. Recurrence method.

The recurrence method relies on a parity check protocol where Alice and Bob compare their local measurement results to determine the quality of their shared entanglement. By verifying the consistency of their outcomes, they can selectively preserve EPR pairs with higher fidelity while discarding those that are likely erroneous. This process effectively suppresses errors, distilling a smaller set of high-purity pairs from a larger, noisy ensemble.

The recurrence protocol consists of the following steps:

1. **Pauli twirling:** Alice and Bob select two noisy pairs. They perform Pauli twirling to transform these states into Bell diagonal states $\rho_{AB} \otimes \sigma_{A'B'}$.
2. **Coupling:** They both perform CNOT operations targeted at the second qubit, effectively transforming their state to

$$\varrho = \text{CNOT}_{AA'} \cdot \text{CNOT}_{BB'}(\rho_{AB} \otimes \sigma_{A'B'}). \quad (\text{A14})$$

3. Measurement: They measure their targeted qubit and compare their results. They keep the control qubit if their measurement outcomes are identical. Otherwise they discard the control qubit.
4. Recurrence: The surviving pairs are then grouped together, and the process is repeated recursively. Each round consumes resources but drives the remaining entanglement closer to a perfect maximally entangled state.

To analyze the performance of this protocol, suppose initially Alice and Bob share states,

$$\varrho_{\text{ini}} = (p_{00} |\Phi^+\rangle\langle\Phi^+| + p_{01} |\Psi^+\rangle\langle\Psi^+| + p_{10} |\Phi^-\rangle\langle\Phi^-| + p_{11} |\Psi^-\rangle\langle\Psi^-|)^{\otimes 2}. \quad (\text{A15})$$

After performing CNOT operations, the state can pass the consistency check if there exists even number of X -errors. The overall probability of passing the check is thus

$$\begin{aligned} p_{\text{pass}} &= p_{00}^2 + p_{01}^2 + p_{10}^2 + p_{11}^2 + 2p_{00}p_{10} + 2p_{01}p_{11} \\ &= (p_{00} + p_{10})^2 + (p_{01} + p_{11})^2. \end{aligned} \quad (\text{A16})$$

The probability of the remaining state being the four Bell states are respectively,

$$\begin{aligned} p_{\Phi^+} &= p_{00}^2 + p_{10}^2, \\ p_{\Psi^+} &= p_{01}^2 + p_{11}^2, \\ p_{\Phi^-} &= 2p_{00}p_{10}, \\ p_{\Psi^-} &= 2p_{01}p_{11}. \end{aligned} \quad (\text{A17})$$

Eq. (A17) could be derived using two very useful identities $\text{CNOT}_{A,B}X_A = X_AX_B\text{CNOT}_{A,B}$ and $\text{CNOT}_{A,B}Z_B = Z_AZ_B\text{CNOT}_{A,B}$. Full table of outcome of different Bell diagonal state in the recurrence protocol could be found in [7]. After normalization of the passing probability p_{pass} , the state after the recurrence protocol would become

$$\rho_{\text{final}} = \frac{p_{00}^2 + p_{10}^2}{p_{\text{pass}}} |\Phi^+\rangle\langle\Phi^+| + \frac{p_{01}^2 + p_{11}^2}{p_{\text{pass}}} |\Psi^+\rangle\langle\Psi^+| + \frac{2p_{00}p_{10}}{p_{\text{pass}}} |\Phi^-\rangle\langle\Phi^-| + \frac{2p_{01}p_{11}}{p_{\text{pass}}} |\Psi^-\rangle\langle\Psi^-|. \quad (\text{A18})$$

When p_{00} itself is high enough, we can always show that $\frac{p_{00}^2 + p_{10}^2}{(p_{00} + p_{10})^2 + (p_{01} + p_{11})^2} > p_{00}$, guaranteeing enhanced fidelity through iteration.

3. Twirling

We introduce the concept of twirling operation and basic properties of it in this part. More details regarding this could be found at [40]. The twirling operation is defined over an ensemble, or put it simple, elements plus probability, of quantum unitary operations, \mathfrak{S} . We consider the following k -th order twirling operation over \mathfrak{S} :

$$\mathcal{T}_{\mathfrak{S}}^k(X) = \mathbb{E}_{U \sim \mathfrak{S}} U^{\otimes k} X U^{\dagger \otimes k}. \quad (\text{A19})$$

where U is drawn from the ensemble \mathfrak{S} and X is the operator being twirled. The expectation is taken over the random unitary operations from \mathfrak{S} .

The mostly commonly seen unitary ensemble for twirling is the Haar random unitaries on a Hilbert space. Intuitively, this is the uniform distribution of all unitaries over a Hilbert space. Suppose X is an operator on the k -fold Hilbert of the Haar random ensemble, then its k -th order twirling satisfying the following equation:

$$\begin{aligned} \mathcal{T}_{\text{Haar}}^{(k)}(X) &= \int_U U^{\otimes k} X U^{\dagger \otimes k} dU \\ &= \sum_{\pi, \sigma \in S_k} \text{Wg}(\pi^{-1}\sigma, d) \text{tr}(X S_{\sigma}^{\dagger}) S_{\pi}, \end{aligned} \quad (\text{A20})$$

where S_k is the permutation group over dimension k . Operator S_{π} is the permutation operator over permutation π . For example if π is a length-2 cycle interchanging system A and B , S_{π} would be the SWAP operator on system AB , which we would also specifically termed as F_{AB} . $\text{Wg}(\sigma, d)$ denotes the Weingarten function for permutation σ over dimension d . For large d , we have $\text{Wg}(1, d) \approx \frac{1}{d^k}$, while other permutations decay as $O(d^{-n-|\pi|})$, where $|\pi|$ is the minimal number of transpositions needed to generate π .

For low order twirling, we can write the expressions in closed form. For example for the first order twirling, we would have:

$$\mathcal{T}_{\text{Haar}}^{(1)}(X) = \text{tr}(X) \frac{\mathbb{I}_d}{d}, \quad (\text{A21})$$

where \mathbb{I}_d is the identity operator with dimension d . The second-order twirling over Haar random ensemble is,

$$\mathcal{T}_{\text{Haar}}^{(2)}(X) = \text{tr}\left(X \frac{\mathbb{I}_{d^2} - d^{-1}F}{d^2 - 1}\right) \mathbb{I}_{d^2} + \text{tr}\left(X \frac{F - d^{-1}\mathbb{I}_{d^2}}{d^2 - 1}\right) F. \quad (\text{A22})$$

Similarly \mathbb{I}_{d^2} is the identity operator on the d^2 -dimension subsystem, and F denotes the SWAP operator on the d^2 -dimension subsystem. This second order twirling is also called bilateral twirling. In our paper, another variant called the mixed bilateral twirling is also considered. The mixed bilateral twirling over a unitary ensemble \mathfrak{S} is

$$\mathcal{N}_{\mathfrak{S}}(X) = \mathbb{E}_{U \sim \mathfrak{S}}(U \otimes U^*) X (U^\dagger \otimes U^T). \quad (\text{A23})$$

The difference of this channel with the ordinary bilateral twirling channel is that it put a complex conjugate on unitaries on the second system. This mixed twirling channel is of particular interest in entanglement distillation because it naturally preserves the EPR pairs.

The Haar random unitary ensemble requires exponential resources to implement in practice. An approximate version of the Haar random unitary ensemble for low order twirling is often used for practical applications. An ensemble \mathfrak{S} is called a unitary k -design if $\mathcal{T}_{\mathfrak{S}}^{(k)} = \mathcal{T}_{\text{Haar}}^{(k)}$. It was shown that the n -qubit Clifford group is an exact unitary 3-design [41, 42]. As we can see in later proof, the most general Hamiltonian twirling requires 4-design unitary ensemble, for which a Clifford group is not enough.

Another very basic twirling operator we would use is the Pauli twirling, defined as

$$\mathcal{T}_{\mathbb{P}}^{(k)}(X) = \sum_{P \in \mathbb{P}} P^{\otimes k} X P^{\otimes k}, \quad (\text{A24})$$

where \mathbb{P} is the group of all Pauli operators in the Hilbert space. One good property of the Pauli channel is that the first order Pauli twirling of an arbitrary quantum channel would makes the channel into a Pauli channel. That is to say, channel $\Lambda_{\mathcal{E}}(\cdot)$, defined as

$$\Lambda_{\mathcal{E}}(\rho) = \sum_{P \in \mathbb{P}} P \mathcal{E}(P \rho P) P \quad (\text{A25})$$

would become a Pauli channel. Here we have abused the notion of twirling a bit by considering the twirling over a channel instead of a state. But the idea of these two kinds of twirling is similar.

In this work, we will use the unitary evolution of Hamiltonian with random time as the unitary ensemble for twirling. For certain Hamiltonian H and a time measure μ , this ensemble could be constructed as $\mathfrak{S}_H = (e^{-iHt}, \mu(t))$. And a major part of this paper is to study the property of mixed bilateral Hamiltonian twirling channel in the form of,

$$\mathcal{N}_H(\rho) = \int_t (e^{-iHt} \otimes e^{iH^*t}) \rho (e^{-iHt} \otimes e^{iH^*t})^\dagger \mu(t). \quad (\text{A26})$$

For readers interested in more materials about the diagonal design induced by eigenvalues of the Hamiltonian, we refer to [26] for more details.

4. Out-of-Time-Order Correlator

In this part, we briefly introduce the definition and basis properties of OTOC.

Definition 3. Consider a Hamiltonian H on a Hilbert space \mathcal{H} . Let ρ be a density matrix also in \mathcal{H} . Let W and V be two Hermitian operators acting on specific subsystems in \mathcal{H} . The Out-of-Time-Order Correlator is defined as

$$\text{OTOC}_{V,W}^H(t) = \text{tr}(\rho \tilde{V}^\dagger W^\dagger \tilde{V} W) \quad (\text{A27})$$

where $\tilde{V} = e^{iHt} V e^{-iHt}$.

In the above definition, ρ is typically chosen as the thermal Gibbs state $\rho = e^{-\beta H} / \text{tr}(e^{-\beta H})$, where $\beta = 1/(k_B T)$ is the inverse temperature. In our case, we would select $\rho = \mathbb{I}/d$ to be the identity. This can also be viewed as a Gibbs state at infinitely high temperature.

OTOC could also be related to commutator, note that $[\tilde{V}, W] = \tilde{V}W - W\tilde{V}$, suppose U and V are unitary operators,

$$\begin{aligned}
\frac{1}{d} \text{tr}([\tilde{V}, W]^\dagger [\tilde{V}, W]) &= \frac{1}{d} \text{tr}\left((W^\dagger \tilde{V}^\dagger - \tilde{V}^\dagger W^\dagger)(\tilde{V}W - W\tilde{V})\right) \\
&= \frac{1}{d} \text{tr}\left(W^\dagger \tilde{V}^\dagger \tilde{V}W - W^\dagger \tilde{V}^\dagger W\tilde{V} - \tilde{V}^\dagger W^\dagger \tilde{V}W + \tilde{V}^\dagger W^\dagger W\tilde{V}\right) \\
&= \frac{1}{d} \text{tr}\left(2I - W^\dagger \tilde{V}^\dagger W\tilde{V} - \tilde{V}^\dagger W^\dagger \tilde{V}W\right) \\
&= 2 - \frac{1}{d} \text{tr}(\tilde{V}^\dagger W^\dagger \tilde{V}W) - \frac{1}{d} \text{tr}\left((\tilde{V}^\dagger W^\dagger \tilde{V}W)^\dagger\right) \\
&= 2 - (\text{OTOC}_{V,W}^H + (\text{OTOC}_{V,W}^H)^*).
\end{aligned} \tag{A28}$$

The last line is due to the fact that $\text{tr}(X) = \text{tr}(X^T)$. Therefore $\text{tr}(X^\dagger) = \text{tr}(X^*) = \text{tr}(X)^*$. This connection shows that lower OTOC directly implies higher non-commutativity.

In the context of quantum information, we often consider the OTOC for two local operators, V and W , acting on spatially separated subsystems. Consider, for example, an n -qubit register where V acts on the first qubit and W on the last. At time $t = 0$, these operators act on disjoint Hilbert spaces and therefore commute, yielding a OTOC value of 1. However, as the system evolves under the Hamiltonian H , the operator $\tilde{V}(t) = e^{iHt} V e^{-iHt}$ undergoes operator spreading. The initially local operator $\tilde{V}(t)$ grows in support, evolving into a complex, non-local operator that eventually overlaps with the support of W . This emerging non-commutativity causes the OTOC value to decay. This phenomenon, known as information scrambling, quantifies how local quantum information is delocalized with the certain Hamiltonian dynamics. This plays a central role in the characterization of complex many-body dynamics as well as a wide range of quantum information tasks.

Appendix B: Some proofs

1. Proof of Theorem 1

Theorem 1 could be proved by simply rewriting all states in the Pauli basis and do a direct calculation. For convenience, we rewrite the Theorem 1 below.

Theorem 1. *Let Alice and Bob share n noisy EPR pairs of the form $|\psi\rangle = (P \otimes I) |\Phi^+\rangle_{AB}^{\otimes n}$, where a Pauli error $P = X_0 Z_0$ acts on Alice's subsystem, with X_0 and Z_0 denoting tensor products of single-qubit Pauli X and Z operators, respectively. Let \mathcal{N}_{H_d} denote the Hamiltonian twirling channel induced by the diagonal Hamiltonian H_d . If $X_0 \neq I$, then the output state after twirling is*

$$\mathcal{N}_{H_d}\left((P \otimes I) |\Phi^+\rangle \langle \Phi^+|^{\otimes n} (P \otimes I)\right) = (X_0 \otimes I) \Delta\left(|\Phi^+\rangle \langle \Phi^+|^{\otimes n}\right) (X_0 \otimes I), \tag{B1}$$

where $\Delta(\cdot)$ denotes the global dephasing channel that removes all off-diagonal terms in the computational basis. If otherwise $X_0 = I$, then the state is invariant under twirling:

$$\mathcal{N}_{H_d}\left((P \otimes I) |\Phi^+\rangle \langle \Phi^+|^{\otimes n} (P \otimes I)\right) = (Z_0 \otimes I) |\Phi^+\rangle \langle \Phi^+|^{\otimes n} (Z_0 \otimes I). \tag{B2}$$

Proof. Eq. (B2) is true because the diagonal Hamiltonian commutes with state $(Z_0 \otimes I) |\Phi^+\rangle \langle \Phi^+|^{\otimes n} (Z_0 \otimes I)$. Therefore for any time t , we always have

$$\begin{aligned}
&(e^{-iH_d t} \otimes e^{iH_d t})(P \otimes I) |\Phi^+\rangle \langle \Phi^+|^{\otimes n} (P \otimes I)(e^{-iH_d t} \otimes e^{iH_d t})^\dagger \\
&= (Z_0 \otimes I)(e^{-iH_d t} \otimes e^{iH_d t}) |\Phi^+\rangle \langle \Phi^+|^{\otimes n} (e^{-iH_d t} \otimes e^{iH_d t})^\dagger (Z_0 \otimes I) \\
&= (Z_0 \otimes I) |\Phi^+\rangle \langle \Phi^+|^{\otimes n} (Z_0 \otimes I).
\end{aligned} \tag{B3}$$

For the $X_0 \neq I$ case, recall Eq. (2) in the main text, we first prove this equation:

$$\begin{aligned}
\mathcal{N}_{H_d}(\rho) &= \sum_{jklm} \int_t (e^{-iH_d t} \otimes e^{iH_d t}) \rho_{jk,lm} |jk\rangle\langle lm| (e^{-iH_d t} \otimes e^{iH_d t})^\dagger \mu(t) \\
&= \sum_{jklm} \int_t e^{-i(\lambda_j - \lambda_k - \lambda_l + \lambda_m)t} \rho_{jk,lm} |jk\rangle\langle lm| \mu(t) \\
&= \sum_{jklm} (\delta_{j,k} \delta_{l,m} + \delta_{j,l} \delta_{k,m} - \delta_{jk} \delta_{jl} \delta_{jm}) \rho_{jk,lm} |jk\rangle\langle lm| \\
&= \sum_{j \neq k} (\rho_{jj,kk} |jj\rangle\langle kk| + \rho_{jk,jk} |jk\rangle\langle jk|) + \sum_j \rho_{jj,jj} |jj\rangle\langle jj|.
\end{aligned} \tag{B4}$$

The only term in a bipartite state $\rho_{jk,lm}$ that can survive under the bilateral Hamiltonian twirling is in the form of $\rho_{jk,jk}$ and $\rho_{jj,kk}$. We rewrite these two kinds of terms in Pauli basis. In this proof, we will stick to the pairwise ordering $\rho_{(AB)^n}$ for convenience, i.e. $2i$ and $2i+1$ -th qubits form an entangled EPR pair that $2i$ -th qubit are hold in Alice's system and $2i+1$ -th qubit are hold in the Bob's system. In this ordering, the diagonal terms $|jk\rangle\langle jk|$ lie in the subspace generated by pure Z -type Pauli operators, i.e. $\langle I, Z \rangle^{\otimes 2n}$. For the terms like $|ii\rangle\langle jj|$, they could be viewed as,

$$|ii\rangle\langle jj| = |ii\rangle\langle ii| (X_{i \oplus j} \otimes X_{i \oplus j}). \tag{B5}$$

In the pairwise ordering, one have

$$\begin{aligned}
|00\rangle\langle 00| &= (II + ZZ + IZ + ZI)/4, \\
|11\rangle\langle 11| &= (II + ZZ - IZ - ZI)/4.
\end{aligned} \tag{B6}$$

Therefore states $\alpha|00\rangle\langle 00| + \beta|00\rangle\langle 11|$ lies in the span of $\langle II + ZZ, IZ + ZI \rangle$. Then it is clear that states in the form $|ii\rangle\langle jj|$ actually lie in the space $\langle II + ZZ, IZ + ZI \rangle^{\otimes n} \times \langle II, XX \rangle^{\otimes n}$. So the Hamiltonian bilateral twirling Λ_H 's effect is equivalent to applying a projection onto the subspaces $\langle I, Z \rangle^{\otimes 2n} + \langle II + ZZ, IZ + ZI \rangle^{\otimes n} \times \langle II, XX \rangle^{\otimes n}$. From these we can conclude that arbitrary indices i and j , one always have:

$$\mathcal{N}_{H_d} \left(((II - ZZ)_{2j, 2j+1} \otimes O_{[2n] \setminus \{2j, 2j+1\}}) \cdot XX_{2i, 2i+1} \right) = 0, \tag{B7}$$

for arbitrary operator O on remaining qubits other than $2j, 2j+1$. Or intuitively, as long as the Pauli combination has structure like $(II - ZZ)XX$, possibly on different sites, it would be projected to 0. Denote I_- to be the indices of qubits where P has X -error on it and $I_+ = n \setminus I_-$. The twirling could thus be written as,

$$\begin{aligned}
&\mathcal{N}_{H_d} \left((P \otimes I) |\Phi^+\rangle\langle \Phi^+|^{\otimes n} (P \otimes I) \right) \\
&= \mathcal{N}_{H_d} \left((\otimes_{i=0}^{n-1} (P_i \otimes I)) |\Phi^+\rangle_{(AB)^n} \langle \Phi^+|_{\otimes_{i=0}^{n-1} (P_i \otimes I)} \right) \\
&= \mathcal{N}_{H_d} \left((\otimes_{i=0}^{n-1} (P_i \otimes I)) \otimes_{i=0}^{n-1} (II + XX)_{2i, 2i+1} \otimes_{i=0}^{n-1} (P_i \otimes I) \right) \\
&= \mathcal{N}_{H_d} (\otimes_{i \in I_-} (II + (-1)^{[P, X_{2i}]} XX)_{2i, 2i+1} \otimes_{i \in I_+} (II + (-1)^{[P, X_{2i}]} XX)_{2i, 2i+1}),
\end{aligned} \tag{B8}$$

where in the second line $P_i = X_{0_i} Z_{0_i}$ means the i -th operator of the Pauli operator P , the last line is obtained by moving the left Pauli operator $\otimes_{i=0}^{n-1} (P_i \otimes I)$ to the right to cancel with the right one and consider the anti-commutation relationship between Paulis. For the case $P = X_0 Z_0$ is not pure Z -type, the index set I_- is non-empty. Any appearance of XX in Eq. (B8) would lead to the Pauli operations of the form $(II - ZZ)_{2j, 2j+1} XX_{2i, 2i+1}$ and thus becomes 0 after applying $\mathcal{N}_{H_d}(D)$ according to Eq. (B7). Therefore the remaining terms are in the form of:

$$\begin{aligned}
\mathcal{N}_{H_d} \left((P \otimes I) |\Phi^+\rangle\langle \Phi^+|^{\otimes n} (P \otimes I) \right) &= \otimes_{i \in I_-} (II - ZZ) \otimes_{i \in I_+} (II + ZZ)_{2i, 2i+1} \\
&= \otimes_{i \in I_-} \frac{|\Psi^+\rangle\langle \Psi^+| + |\Psi^-\rangle\langle \Psi^-|}{2} \otimes_{i \in I_+} \frac{|\Phi^+\rangle\langle \Phi^+| + |\Phi^-\rangle\langle \Phi^-|}{2} \\
&= X_0 \Delta(|\Phi^+\rangle\langle \Phi^+|) X_0.
\end{aligned} \tag{B9}$$

□

2. Proof of Lemma 1

Lemma 1. Consider a Hamiltonian distillation protocol for n noisy EPR pairs $\Lambda(|\Phi^+\rangle\langle\Phi^+|^{\otimes n})$ subject to Pauli error $\Lambda(\rho) = \sum_{P \in \mathcal{P}} c_P P \rho P$ on Alice's system. Hamiltonian H together with a time ensemble μ is adopted to produce the channel \mathcal{N}_H in the twirling step. Error detection is implemented by Alice measuring a POVM $M = \{M_x\}$ and Bob measuring the conjugate $M^* = \{M_x^*\}$ on m qubits, chosen such that $\sum_x \text{Tr}(M_x \otimes M_x^* |\Phi^+\rangle\langle\Phi^+|^{\otimes n}) = 1$. The outcome corresponding to $I - \sum_x M_x \otimes M_x^*$ is interpreted as detected error and discarded. After post-selection, the output fidelity f_{output} and yield Y are given by

$$\begin{aligned} f_{\text{output}} &= \frac{1}{1 + \text{OTOC}_{\Lambda, M}^{\mathcal{N}_H} / c_I}, \\ Y &= (c_I + \text{OTOC}_{\Lambda, M}^{\mathcal{N}_H})(1 - m/n). \end{aligned} \quad (\text{B10})$$

Here c_I is the probability of obtaining identity channel in noise Λ . The averaged OTOC is defined as

$$\text{OTOC}_{\Lambda, M}^{\mathcal{N}_H} = \int_t \sum_{P \in \mathcal{P} \setminus I} \sum_x c_P \text{OTOC}_{P, M_x}^{e^{-iHt}} \cdot \mu(t). \quad (\text{B11})$$

Proof. We define error detection rate R as the ratio of the probability of obtaining distinct outcomes in the error detection step to the total probability of Pauli errors occurring. Suppose after Hamiltonian twirling the error detection rate is R for Pauli channel Λ where the probability of the identity channel is c_I , the fidelity and yield of the post-selected state is then given by

$$\begin{aligned} f_{\text{out}} &= \frac{c_I}{(c_I + (1 - c_I)(1 - R))}, \\ Y &= (c_I + (1 - c_I)(1 - R))(1 - m/n). \end{aligned} \quad (\text{B12})$$

Since the Pauli noise could be viewed as classical mixture of different Pauli error. We only need to consider the error detection probability of each Pauli error individually. Then gathering all individual results we are able to compute the final yield and fidelity.

Suppose the EPR states suffer a Pauli error P on Alice's system. The probability of detecting errors could be expressed as

$$\begin{aligned} p(P, t) &= \langle \Phi^+ |^{\otimes n} (P \otimes I) (e^{-iHt} \otimes e^{iH^*t}) (I - \sum_x M_x \otimes M_x^*) (e^{-iHt} \otimes e^{iH^*t})^\dagger (P \otimes I) | \Phi^+ \rangle^{\otimes n} \\ &= 1 - \sum_x \langle \Phi^+ |^{\otimes n} (P \otimes I) (e^{-iHt} \otimes e^{iH^*t}) (M_x \otimes M_x^*) (e^{-iHt} \otimes e^{iH^*t})^\dagger (P \otimes I) | \Phi^+ \rangle^{\otimes n} \\ &= 1 - \sum_x \text{tr} \left(e^{iHt} P e^{-iHt} M_x e^{iHt} P e^{-iHt} M_x \right) \\ &= 1 - \sum_x \text{OTOC}_{P, M_x}^{e^{-iHt}}. \end{aligned} \quad (\text{B13})$$

The third line is because $\langle \Phi^+ |^{\otimes n} A \otimes B | \Phi^+ \rangle^{\otimes n} = \text{tr}(AB^T)$. Averaging over time ensemble μ and all Pauli errors, we can obtain the error detection rate as

$$\begin{aligned} R &= \frac{\int_t \sum_{P \in \mathcal{P} \setminus I} \sum_x c_P (1 - \sum_x \text{OTOC}_{P, M_x}^{e^{-iHt}}) \mu(t)}{1 - c_I} \\ &= \frac{1 - c_I - \text{OTOC}_{\Lambda, M}^{\mathcal{N}_H}}{1 - c_I}. \end{aligned} \quad (\text{B14})$$

Take this into Eq. (B12) proves this theorem. \square

3. Proof of Theorem 2

Theorem 2. Consider a Hamiltonian distillation protocol for n noisy EPR pairs $\Lambda(|\Phi^+\rangle\langle\Phi^+|^{\otimes n})$ subject to Pauli noise $\Lambda(\rho) = \sum_{P \in \mathcal{P}} c_P P \rho P$ on Alice's system, with probability of identity channel being c_I . Consider a n -qubit Hamiltonian

be $H = UDU^\dagger$, where U is drawn from the Haar measure in the twirling step. After Hamiltonian twirling with H and measuring m qubit pairs in the computational basis, the output fidelity and yield converge, in the large n limit, to

$$\begin{aligned} f_{\text{out}} &= \frac{c_I}{c_I + 2^{-m}(1 - c_I)}, \\ Y &= (c_I(1 - 2^{-m}) + 2^{-m})(1 - m/n). \end{aligned} \quad (\text{B15})$$

Proof. Throughout this proof, we use $|\Phi^+\rangle = \sum_{i=0}^{d-1} |ii\rangle$ to denote the unnormalized EPR state (typically $d = 2^n$). We will specifically add a $1/\sqrt{d}$ factor to denote the quantum state. For the m -qubit computational basis measurement, the identical outcomes corresponds to the projector

$$\Pi_{id} = \sum_{i=0}^{2^m-1} |ii\rangle\langle ii| \otimes I^{\otimes 2(n-m)}. \quad (\text{B16})$$

The distinct outcomes, representing the event of detecting an error, thus corresponds to the projector

$$\Pi = I - \Pi_{id} = I^{\otimes 2n} - \sum_{i=0}^{2^m-1} |ii\rangle\langle ii| \otimes I^{\otimes 2(n-m)}. \quad (\text{B17})$$

For arbitrary bipartite state ρ , $\text{tr}(\Pi\rho)$ indicates the probability that an error is detected for the state. Since we assume the noise channel is a Pauli channel, we only need to account for each Pauli error individually.

Consider a Pauli error P , we first express the error detection probability for EPR state affected by this error P on Alice's side, which is

$$\begin{aligned} p(P) &= \frac{1}{d} \text{tr} \left(\Pi (U \otimes U^*) (e^{-iDt} \otimes e^{iDt}) (U^\dagger \otimes U^T) (P \otimes I) |\Phi^+\rangle\langle\Phi^+| (P \otimes I) (U \otimes U^*) (e^{iDt} \otimes e^{-iDt}) (U^\dagger \otimes U^T) \right) \\ &= \frac{1}{d} \langle\Phi^+| (P \otimes I) (U \otimes U^*) (e^{iDt} \otimes e^{-iDt}) (U^\dagger \otimes U^T) \Pi (U \otimes U^*) (e^{-iDt} \otimes e^{iDt}) (U^\dagger \otimes U^T) (P \otimes I) |\Phi^+\rangle. \end{aligned} \quad (\text{B18})$$

To better understand the twirling effect, we rewrite it into the 4-twirling form,

$$\begin{aligned} p(P) &= \frac{1}{d} \langle\Phi^+|_{12} \langle\Phi^+|_{34} (PUe^{iDt}U^\dagger) \otimes (U^*e^{-iDt}U^T) \otimes (I \otimes P) \cdot (Ue^{-iDt}U^\dagger \otimes U^*e^{iDt}U^T)^T \cdot \Pi_{1,2} \cdot |\Phi^+\rangle_{13} |\Phi^+\rangle_{24} \\ &= \frac{1}{d} \langle\Phi^+|_{12} \langle\Phi^+|_{34} PUe^{iDt}U^\dagger \otimes U^*e^{-iDt}U^T \otimes U^*e^{-iDt}U^T \otimes PUe^{iDt}U^\dagger \cdot \Pi_{1,2} \cdot |\Phi^+\rangle_{13} |\Phi^+\rangle_{24}, \end{aligned} \quad (\text{B19})$$

where the subscripts means the system that bipartite operator affects. This equation is also shown in Fig 7 for visual understanding.

The key point here is to understand the 4-twirling $Ue^{iDt}U^\dagger \otimes U^*e^{-iDt}U^T \otimes U^*e^{-iDt}U^T \otimes Ue^{iDt}U^\dagger$, or the red box in Figure 7. Consider the average of error detection probability over time ensemble μ and the Haar random unitary U , we would obtain:

$$\begin{aligned} &\int_t \int_U (U \otimes U^* \otimes U^* \otimes U) (e^{iDt} \otimes e^{-iDt} \otimes e^{-iDt} \otimes e^{iDt}) (U^\dagger \otimes U^T \otimes U^T \otimes U^\dagger) dU dt \\ &= \left(\int_{U,t} U^{\otimes 4} (e^{iDt} \otimes e^{-iDt} \otimes e^{-iDt} \otimes e^{iDt}) U^{\dagger \otimes 4} \mu(t) dU \right)^{T_2, T_3}. \end{aligned} \quad (\text{B20})$$

The above equation is because e^{iDt} is diagonal, thus $e^{iDt^T} = e^{iDt}$. The inner term $U^{\otimes 4} (e^{iDt} \otimes e^{-iDt} \otimes e^{-iDt} \otimes e^{iDt}) U^{\dagger \otimes 4}$ is a standard 4-twirling as introduced in Sec A 3. We rewrite it here as

$$\int_U U^{\otimes 4} O U^{\dagger \otimes 4} dU = \sum_{\pi, \sigma \in S_4} Wg(\pi^{-1}\sigma, d) S_\pi \text{tr}(O S_\sigma^\dagger). \quad (\text{B21})$$

For our case $O = \int_t (e^{iDt} \otimes e^{-iDt} \otimes e^{-iDt} \otimes e^{iDt}) \mu(t)$. To compute Eq. (B20), we first compute the trace between

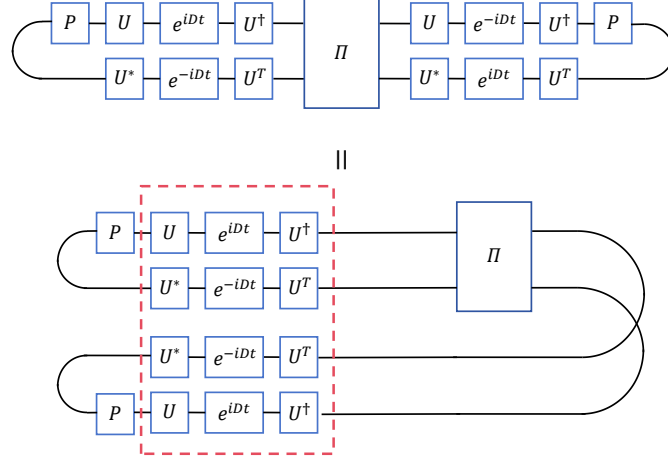


FIG. 7. Conversion to 4-twirling

different permutation S_σ and the operator O :

$$\begin{aligned}
 & \text{tr} \left(\int_t (e^{iDt} \otimes e^{-iDt} \otimes e^{-iDt} \otimes e^{iDt}) S_\sigma dt \right) \\
 & \left\{ \begin{array}{l} \int_t \text{tr}(e^{-iDt})^2 \text{tr}(e^{iDt})^2 dt, \sigma = (1, 1, 1, 1) \\ \int_t \text{tr}(I) \text{tr}(e^{-iDt}) \text{tr}(e^{iDt}) dt, \sigma = (2, 1, 1) \text{ with 2-cycle on } e^{iDt} \text{ and } e^{-iDt} \\ \int_t \text{tr}(e^{\pm 2iDt}) \text{tr}(e^{\mp iDt})^2 dt, \sigma = (2, 1, 1) \text{ with 2-cycle on same sign} \\ \int_t \text{tr}(I)^2 dt, \sigma = (2, 2) \text{ with both cycle on } e^{iDt} \text{ and } e^{-iDt} \\ \int_t \text{tr}(e^{2iDt}) \text{tr}(e^{-2iDt}) dt, \sigma = (2, 2) \text{ with both cycle on same sign} \\ \int_t \text{tr}(e^{-iDt}) \text{tr}(e^{iDt}) dt, \sigma = (3, 1) \\ \int_t \text{tr}(I) dt, \sigma = (4) \end{array} \right. , \tag{B22}
 \end{aligned}$$

where notations like $(2, 1, 1)$ is the partition notation meaning that the permutation could be divided into one 2-cycle and two 1-cycle. We compute the average trace for each case,

1. $\sigma = (1, 1, 1, 1)$:

$$\begin{aligned}
 & \int_t \text{tr}(e^{-iDt})^2 \text{tr}(e^{iDt})^2 \\
 & = \int_t \left(\sum_j e^{-id_j t} \right)^2 \left(\sum_j e^{id_j t} \right)^2 \\
 & = \int_t \sum_{j,k,l,m} e^{i(d_j+d_k-d_l-d_m)t} \\
 & = \sum_{j,k,l,m} \delta_{jl} \delta_{km} + \delta_{jm} \delta_{kl} - \delta_{jk} \delta_{jl} \delta_{jm} \\
 & = 2d^2 - d \tag{B23}
 \end{aligned}$$

2. $\sigma = (2, 1, 1)$ with 2-cycle on e^{iDt} and e^{-iDt} :

$$\begin{aligned} & \int_t \text{tr}(I) \text{tr}(e^{-iDt}) \text{tr}(e^{iDt}) dt \\ &= d \cdot \sum_{ij} \delta_{ij} \\ &= d^2 \end{aligned} \tag{B24}$$

3. $\sigma = (2, 1, 1)$ with 2-cycle on same sign:

$$\begin{aligned} & \int_t \text{tr}(e^{\pm 2iDt}) \text{tr}(e^{\mp iDt})^2 dt \\ &= \int_t \sum_{jkl} e^{i(2d_j - d_k - d_l)t} dt \\ &= \sum_{jkl} \delta_{jk} \delta_{jl} \\ &= d \end{aligned} \tag{B25}$$

4. $\sigma = (2, 2)$ with both cycle on e^{iDt} and e^{-iDt} :

$$\int_t \text{tr}(I)^2 dt = d^2 \tag{B26}$$

5. $\sigma = (2, 2)$ with both cycle on same sign:

$$\begin{aligned} & \int_t \text{tr}(e^{2iDt}) \text{tr}(e^{-2iDt}) dt \\ &= \int_t \sum_{jk} e^{2i(d_j - d_k)t} dt \\ &= \sum_{jk} \delta_{jk} \\ &= d \end{aligned} \tag{B27}$$

6. $\sigma = (3, 1)$:

$$\int_t \text{tr}(e^{-iDt}) \text{tr}(e^{iDt}) dt = d \tag{B28}$$

7. $\sigma = (4)$:

$$\int_t \text{tr}(I) dt = d \tag{B29}$$

The full computation of Eq. (B20) would be tedious. For simplicity we only consider approximation in the large d limit. In this case we know that [43]

$$\begin{aligned} Wg(1^4, d) &\approx d^{-4} \\ Wg(21^2, d) &\approx -d^{-5} \\ Wg(31, d) &\approx 2d^{-6} \\ Wg(2^2, d) &\approx d^{-6} \\ Wg(4, d) &\approx -5d^{-7}. \end{aligned} \tag{B30}$$

Combine Eq. (B30) and Eqs. (B23)–(B29) one can have a approximation of Eq. (B20) in the large d limit. Note that now Eq. (B20) would have the form of $\sum_{S_\sigma \in S_4} f(S_\sigma, d) S_\sigma^{T_2 T_3}$ where $f(S_\sigma, d)$ is a scalar function related to S_σ and dimension d . Finally to compute the error detection probability, the time ensemble and Haar random average of Eq. (B19) which could be expressed as below:

$$p_{all} = \frac{1}{d} \langle \Phi^+ |_{12} \langle \Phi^+ |_{34} P_1 P_4 \left(\sum_{\pi, \sigma \in S_4} Wg(\pi^{-1}\sigma, d) S_\pi \text{tr} \left(\int_t (e^{iDt} \otimes e^{-iDt} \otimes e^{-iDt} \otimes e^{iDt}) \mu(t) S_\sigma^\dagger \right) \right) \Pi_{12} |\Phi^+\rangle_{13} |\Phi^+\rangle_{24} \tag{B31}$$

we have to evaluate the terms $\langle \Phi^+ |_{12} \langle \Phi^+ |_{34} P_1 P_4 S_\pi^{T_2 T_3} \Pi_{12} | \Phi^+ \rangle_{13} | \Phi^+ \rangle_{24}$. The value of this quantity could be classified into following categories:

- 0, for permutation (12); (34); (12)(34); (123); (124); (143); (243); (1234); (1243); (1432). As shown in Figure 8, this is the case where factor $\text{tr}(P)$ occurs. Since $\text{tr}(P) = 0$ for any Pauli error, no matter what the leftover black box is, the overall value is 0.

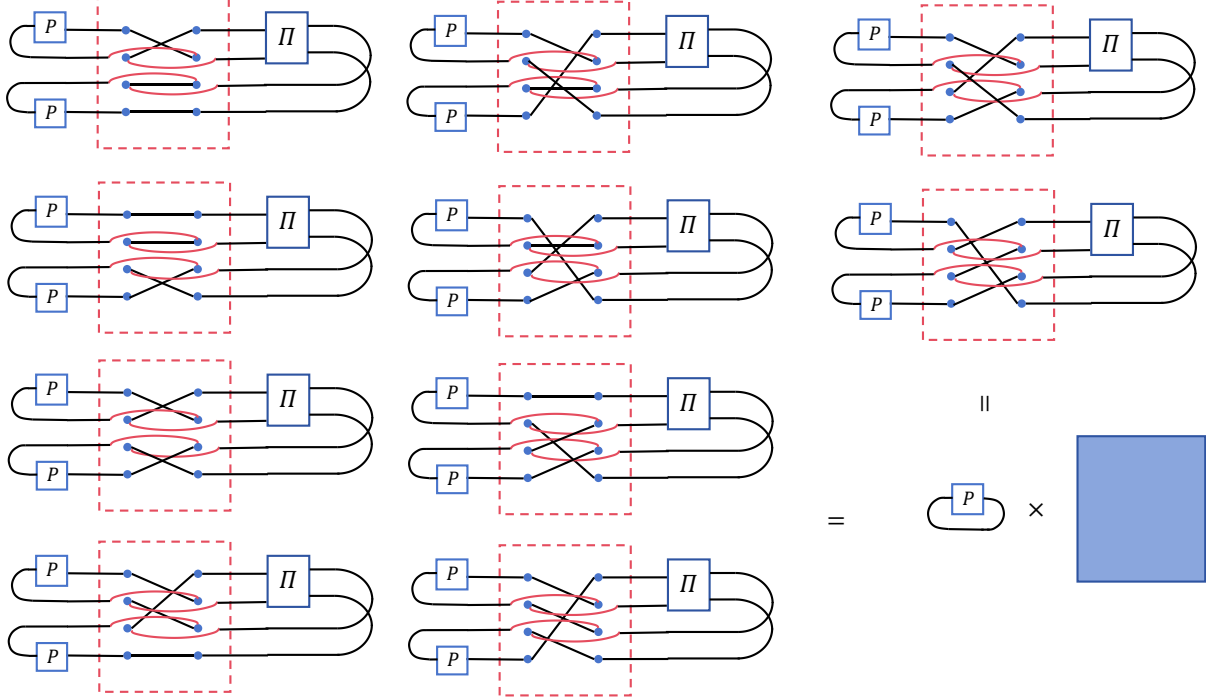


FIG. 8. case1

- $d(1 - x_p)$, for permutation $(1^4); (14)(23)$; This case occurs when the trace can be expressed in Figure 9. In

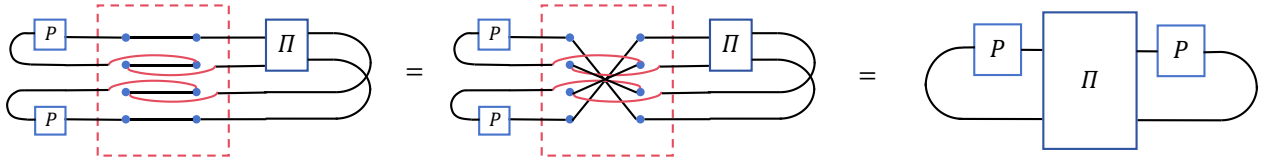


FIG. 9. case2

this case the trace should be

$$\langle \Phi^+ | I - \sum_{i=0}^{2^m-1} P_1 |ii\rangle \langle ii| \otimes I^{\otimes 2(n-m)} P_1 | \Phi^+ \rangle = d - \sum_{i=0}^{2^m-1} \langle \Phi^+ | P_1 |ii\rangle \langle ii| \otimes I^{\otimes 2(n-m)} P_1 | \Phi^+ \rangle. \quad (\text{B32})$$

The latter term is 0 if P has X on the first m qubits and d if not. So this trace is $d(1 - x_p)$ depending on whether $x_p = 0$ (P have X on first m qubits) or not.

3. $d^2(1 - 2^{-m})$, for permutation (13); (24); (1324); (1423) This is the cases where factor in Figure 10 occurs. And we have

$$\text{tr}(\Pi) = 2^{2n} - 2^m \cdot 2^{2(n-m)} = 2^{2n}(1 - 2^{-m}) = d^2(1 - 2^{-m}) \quad (\text{B33})$$

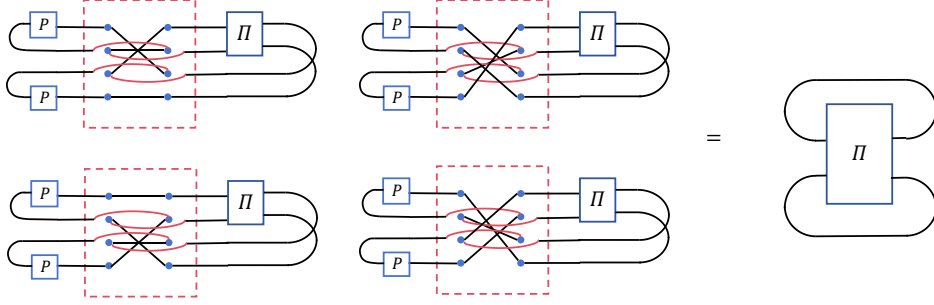


FIG. 10. case3

4. 0, for permutations (132); (142); (134); (234). This is the case shown in Figure 11 where we have the following expression:

$$\langle \Phi^+ | \Pi | \Phi^+ \rangle = 0 \quad (\text{B34})$$

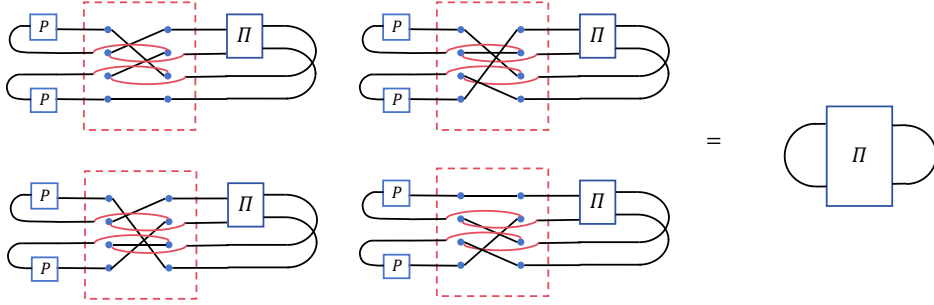


FIG. 11. case4

5. $\pm y \cdot d^2 2^{-m}$, for permutation (14); (23) This is the cases where factor in Figure 12 occurs. This time we have,

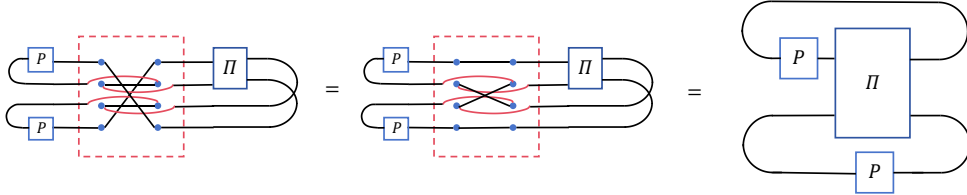


FIG. 12. case5

$$\begin{aligned} \text{tr}(P \otimes P^T \Pi) &= \pm \text{tr}(P^{\otimes 2} \Pi) \\ &= \pm \text{tr}(P^{\otimes 2}) \mp \sum_i \text{tr}(P^{\otimes 2} |ii\rangle\langle ii| \otimes I^{2(n-m)}) \end{aligned} \quad (\text{B35})$$

The first term is obviously 0. The second term is nonzero only if P is I on all $2(n-m)$ qubits and is pure Z -type in the $2m$ qubits. We use y to denote whether this case is satisfied or not. Then this trace could be expressed as $\pm y \cdot d^2 2^{-m}$.

6. $d^3(1 - 2^{-m})$, for permutation (13)(24). This is a very special case where the trace is as in Figure 13. It is

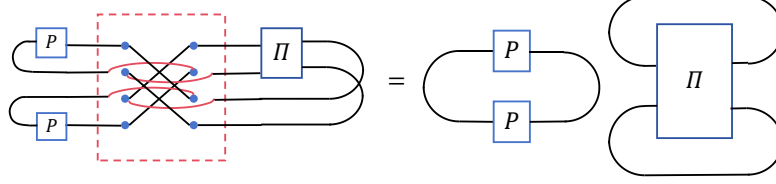


FIG. 13. case6

$d^2(1 - 2^{-m})$ multiply with another d obtained from the left circle.

7. 0, for permutation (1342). This time the trace is as in Figure 14. The trace is 0 due to the structure of $\langle \Phi^+ | \Pi | \Phi^+ \rangle$.

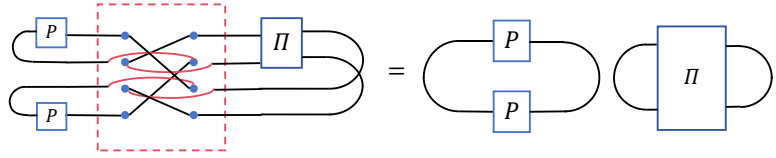


FIG. 14. case7

The leading term of Eq. (B31) in the large n limit should be the one that maximize all three of the Weingarten function $Wg(\pi^{-1}\sigma, d)$, the trace between diagonal matrices and permutation $\text{tr}(\int_t (e^{-iDt} \otimes e^{iDt} \otimes e^{iDt} \otimes e^{-iDt}) S_\sigma^\dagger dt)$, and the error detection probability trace $\langle \Phi^+ |_{12} \langle \Phi^+ |_{34} P_1 \otimes P_4 S_\pi^{T_2 T_3} \Pi_{12} | \Phi^+ \rangle_{13} | \Phi^+ \rangle_{24}$. And actually there is exactly one such (π, σ) pair that simultaneously maximize all these three terms. First note that for Weingarten function only $Wg(1^4, d) \approx d^{-4}$ while others are smaller in magnitude. This restricts $\sigma = \pi$. Then consider $\langle \Phi^+ |_{12} \langle \Phi^+ |_{34} P_1 \otimes P_4 S_\pi^{T_2 T_3} \Pi_{12} | \Phi^+ \rangle_{13} | \Phi^+ \rangle_{24}$, the only one with d^3 scaling is (13)(24). Also note that (13)(24) in the $\text{tr}(\int_t (e^{-iDt} \otimes e^{iDt} \otimes e^{iDt} \otimes e^{-iDt}) S_\sigma dt)$ also gives the d^2 scaling. One can verify that this is the only pair that maximize all these three terms. So in the large d limit, we only need to count the contribution merely from this term, which is,

$$\begin{aligned} p_{all} &\approx \frac{1}{d} \frac{1}{d^4} d^3 (1 - 2^{-m}) \cdot d^2 + O(d^{-1}) \\ &\approx 1 - 2^{-m} + O(d^{-1}). \end{aligned} \quad (\text{B36})$$

Since this relationship holds independent of what Pauli error P is, we can conclude that the fidelity and yield should converge to,

$$\begin{aligned} f_{\text{out}} &= \frac{c_I}{c_I + (1 - c_I)(1 - 2^{-m})}, \\ Y &= (c_I + 2^{-m}(1 - c_I))(1 - m/n), \end{aligned} \quad (\text{B37})$$

in the large d , or equivalently n , limit. □

4. Proof of Theorem 3

Theorem 3. Consider a Hamiltonian distillation protocol for n EPR pairs $|\Phi^+\rangle_{AB}^{\otimes n}$, each subjected to i.i.d. local depolarizing noise of strength p on Alice's side. Let a Hamiltonian distillation protocol be applied with the following choices: the Hamiltonian used in the twirling step is of the form $H = CDC^\dagger$, where C is drawn from the Clifford group

and D is diagonal. The error-detection step is implemented via a projective measurement defined by the orthogonal projectors $\left\{C \left(\prod_{j=1}^m \frac{I+(-1)^{s_j} X_j}{2}\right) \otimes I^{\otimes(n-m)} C^\dagger : \vec{s} \in \{0,1\}^m\right\}$. The output fidelity could be lower bounded by:

$$f_{\text{out}} \geq \frac{1}{1 + (\Delta + 2^{-m}(1 - \Delta - (1 - 3p/4)^n)) / (1 - 3p/4)^n}. \quad (\text{B38})$$

Here Δ is defined for an arbitrary integer parameter $d \leq n$, given by:

$$\Delta = 2^{-n \left(1 - H(d/n) - d/n \log_2 3 - \delta\right)} + 2^{-n \left(\log_2 \frac{2}{4-3p} + d/n \log_2 \frac{4-3p}{p}\right)}. \quad (\text{B39})$$

where $H(\cdot)$ denotes the binary entropy function, and $\delta > 0$ is an arbitrarily small constant.

Proof. When the diagonalizing unitary of Hamiltonian is a Clifford gate C , the Pauli operators in the set $\mathbf{P}_{ud} = C\{I, Z\}^{\otimes n} C^\dagger \setminus I^{\otimes n}$ actually commutes with the Hamiltonian. The Pauli operators in this set becomes hard to detect because they cannot be scrambled. We first bound the probability of the operators in \mathbf{P}_{ud} occurring. For certain C in Clifford group, using $\omega(d)$ to denote the set of all non-identity Pauli operators whose weight is smaller than d , the probability of occurring Pauli operators in \mathbf{P}_{ud} whose weight is smaller than d could be written as,

$$\begin{aligned} p_{lw}(C) &= \Pr\{\exists \sigma \in \langle I, Z \rangle^{\otimes n} \setminus I^{\otimes n}, \exists \nu \in \omega(d), \text{tr}(\nu C \sigma C^\dagger) \neq 0\} \\ &\leq \sum_{\sigma \in \langle I, Z \rangle^{\otimes n} \setminus I^{\otimes n}} \sum_{\nu \in \omega(d)} \Pr\{\text{tr}(\nu C \sigma C^\dagger) \neq 0\} \\ &= \frac{1}{2^n} \sum_{\sigma \in \langle I, Z \rangle^{\otimes n} \setminus I^{\otimes n}} \sum_{\nu \in \omega(d)} |\text{tr}(\nu C \sigma C^\dagger)| \\ &= \frac{1}{4^n} \sum_{\sigma \in \langle I, Z \rangle^{\otimes n} \setminus I^{\otimes n}} \sum_{\nu \in \omega(d)} \text{tr}(\nu^{\otimes 2} C^{\otimes 2} \sigma^{\otimes 2} C^{\dagger \otimes 2}) \end{aligned} \quad (\text{B40})$$

The second line is by the union bound and the third line is due to the fact that non-traceless $\nu C \sigma C^\dagger$ must be $\pm I$. The final line is by the property that $\text{tr}(A \otimes B) = \text{tr}(A) \cdot \text{tr}(B)$. Therefore the probability of occurring low weight Pauli operators, after average on the whole Clifford group, becomes

$$\begin{aligned} \mathbb{E}_C[p_{lw}(C)] &\leq \frac{1}{4^n} \mathbb{E}_C \left[\sum_{\sigma \in \langle I, Z \rangle^{\otimes n} \setminus I^{\otimes n}} \sum_{\nu \in \omega(d)} \text{tr}(\nu^{\otimes 2} C^{\otimes 2} \sigma^{\otimes 2} C^{\dagger \otimes 2}) \right] \\ &= \frac{1}{4^n} \sum_{\sigma \in \langle I, Z \rangle^{\otimes n} \setminus I^{\otimes n}} \sum_{\nu \in \omega(d)} \text{tr} \left(\nu^{\otimes 2} \frac{-2^n I + 4^n F}{2^n (4^n - 1)} \right) \\ &= \frac{1}{4^n} \cdot (2^n - 1) \cdot |\omega(d)| \cdot \frac{4^n}{4^n - 1} \\ &= \frac{2^n - 1}{4^n - 1} \cdot \sum_{i=m}^d \binom{n}{m} 3^m \end{aligned} \quad (\text{B41})$$

Suppose $d = k \cdot n$ for some $k < 3/4$, then by the Shannon's coding theory, in the large n limit we will have

$$\sum_{m=1}^d \binom{n}{m} 3^m \leq 2^{n \left(H(k) + k \log_2 3 + \delta\right)}, \quad (\text{B42})$$

for some arbitrarily small constant $\delta > 0$ where $H(x) = -x \log x - (1-x) \log(1-x)$ is the Shannon entropy. Therefore we can bound the average low weight probability as

$$\mathbb{E}_C[p_{lw}(C)] \leq 2^{-n(1-H(d/n)-d/n \log_2 3 - \delta)} \quad (\text{B43})$$

The term $(1 - H(d/n) - d/n \log_2 3)$ is larger than 0 for any d/n smaller than 0.55. For local depolarizing noise with noise strength p , the occurring probability of this set \mathbf{P}_{ud} can be bounded as,

$$\begin{aligned} \Pr\{\mathbf{P}_{ud}\} &\leq \Pr\{\exists \sigma \in \langle I, Z \rangle^{\otimes n} \setminus I^{\otimes n}, |C \sigma C^\dagger| \leq d\} \\ &\quad + \Pr\{C \langle I, Z \rangle^{\otimes n} C^\dagger \setminus I^{\otimes n} \wedge \forall \sigma \in \langle I, Z \rangle^{\otimes n} \setminus I^{\otimes n}, |C \sigma C^\dagger| > d\} \\ &\leq 2^{-n \left(1 - H(d/n) - d/n \log_2 3 - \delta\right)} + 2^n \left(\frac{p}{4}\right)^d \left(1 - \frac{3p}{4}\right)^{n-d} \\ &= 2^{-n \left(1 - H(d/n) - d/n \log_2 3 - \delta\right)} + 2^{-n \left(\log_2 \frac{2}{4-3p} + d/n \log_2 \frac{4-3p}{p}\right)} \end{aligned} \quad (\text{B44})$$

The second line is due to Eq. (B43) and the condition that all elements have weights larger than d in the second term. For error $P \notin \mathcal{P}_{ud}$, define the error projector to be

$$\Pi = I - \sum_{\vec{s} \in \{0,1\}^m} \left(C \left(\prod_{j=1}^m \frac{I + (-1)^{s_j} X_j}{2} \right) \otimes I^{\otimes(n-m)} C^\dagger \right) \otimes \left(C^* \left(\prod_{j=1}^m \frac{I + (-1)^{s_j} X_j}{2} \right) \otimes I^{\otimes(n-m)} C^T \right) \quad (\text{B45})$$

the probability of it being detected is,

$$\begin{aligned} p(P) &= \int_t \text{tr} \left(\Pi (C \otimes C^*) (e^{-iDt} \otimes e^{iDt}) (C^\dagger \otimes C^T) (P \otimes I) |\Phi^+ \rangle \langle \Phi^+|^{\otimes n} (P \otimes I) (C \otimes C^*) (e^{iDt} \otimes e^{-iDt}) (C^\dagger \otimes C^T) \right) \mu(t) \\ &= 1 - \int_t \sum_{\vec{s} \in \{0,1\}^m} \text{tr} \left(\left(\prod_{j=1}^m \frac{I + (-1)^{s_j} X_j}{2} \right)^{\otimes 2} (e^{-iDt} \otimes e^{iDt}) (C^\dagger P C \otimes I) |\Phi^+ \rangle \langle \Phi^+|^{\otimes n} (C^\dagger P C \otimes I) (e^{iDt} \otimes e^{-iDt}) \right) \mu(t). \end{aligned} \quad (\text{B46})$$

Since $C^\dagger P C$ is not pure Z -type, applying Theorem 1, we could obtain,

$$\begin{aligned} p(P) &= 1 - \sum_{\vec{s} \in \{0,1\}^m} \text{tr} \left(\left(\prod_{j=1}^m \frac{I + (-1)^{s_j} X_j}{2} \right)^{\otimes 2} (X_p \otimes I) \Delta (|\Phi^+ \rangle \langle \Phi^+|^{\otimes n}) (X_p \otimes I) \right) \\ &= 1 - 2^{-m}. \end{aligned} \quad (\text{B47})$$

The second line is because among all errors in $\Delta(\cdot)$, only the identity channel can produce nonzero trace with $\left(\prod_{j=1}^m \frac{I + (-1)^{s_j} X_j}{2} \right)^{\otimes 2}$, which occurs with probability only 2^{-m} . Combined Eq. (B44) and Eq. (B47) we could bound the fidelity by:

$$\begin{aligned} f_{\text{out}} &= \frac{(1 - 3p/4)^n}{(1 - 3p/4)^n + (1 - R_{ud}) \cdot \Pr\{\mathcal{P}_{ud}\} + 2^{-m}(1 - (1 - 3p/4)^n - \Pr\{\mathcal{P}_{ud}\})} \\ &\geq \frac{(1 - 3p/4)^n}{(1 - 3p/4)^n + \Pr\{\mathcal{P}_{ud}\} + 2^{-m}(1 - (1 - 3p/4)^n - \Pr\{\mathcal{P}_{ud}\})} \\ &\geq \frac{(1 - 3p/4)^n}{(1 - 3p/4)^n + \Delta + 2^{-m}(1 - (1 - 3p/4)^n - \Delta)}, \end{aligned} \quad (\text{B48})$$

where $R_{ud} \in [0,1]$ is the detection rate of set \mathcal{P}_{ud} and Δ is defined in Eq. (B39). The third line is simply due to Eq. (B44). \square

To check whether the fidelity could be exponentially close to 1, we basically need to focus on the term

$$\frac{\Delta}{(1 - 3p/4)^n} = 2^{n \left(\log_2 \frac{4}{4-3p} - 1 + H(d/n) + d/n \log_2 3 + \delta \right)} + 2^{n \left(1 - d/n \log \frac{4-3p}{p} \right)}. \quad (\text{B49})$$

Numerics show that take $d/n = 0.16$, when $p \leq 6.5\%$, both $\left(\log_2 \frac{4}{4-3p} - 1 + H(d/n) + d/n \log_2 3 + \delta \right)$ and $\left(1 - d/n \log \frac{4-3p}{p} \right)$ can be less than 0. Therefore the fidelity could be exponentially close to 1 in the large n limit.

5. Proof of Theorem 4

Theorem 4. Consider an entanglement-based QKD protocol between Alice and Bob. Assume that the shared EPR pairs are subjected to local i.i.d. depolarizing noise of strength p on Bob's side. Alice and Bob group the noisy pairs into blocks of size n and perform Hamiltonian twirling using a diagonal Hamiltonian. They then measure m qubit pairs in the Hadamard basis for error detection. The surviving qubit of error detection are measured in the computational basis to generate key bits, followed by standard privacy amplification. The resulting secret key rate is given by:

$$R = \left(\left(1 - \frac{3}{4}p \right)^m \left(1 - \frac{p}{2} \right)^{n-m} + 2^{-m} \left(1 - \left(1 - \frac{p}{2} \right)^n \right) \right) (1 - H(e_p)) (1 - m/n), \quad (\text{B50})$$

where $H(\cdot)$ denotes the Shannon entropy and $e_p = \frac{2^{-(m+1)}(1-(\frac{p}{2})^n) + \frac{p}{4 \cdot 2^p}(1-\frac{3p}{4})^m(1-\frac{p}{2})^{n-m}}{2^{-m}(1-(1-\frac{p}{2})^n) + (1-\frac{3p}{4})^m(1-\frac{p}{2})^{n-m}}$ is the effective phase error rate inferred from the error-detection step. This protocol tolerates local depolarizing noise up to a threshold p_{tol} , where $p_{tol} \in [0, 2/3]$ is the solution to

$$\left(1 - \frac{p}{2}\right)^{1-\frac{m}{n}} \left(2 - \frac{3p}{2}\right)^{\frac{m}{n}} = 1. \quad (\text{B51})$$

Proof. We first consider the error detection step. States surviving this step and their corresponding surviving probability are listed below:

1. Pure EPR states: The initial probability of pure EPR state is $(1 - \frac{3p}{4})^n$. They pass the error detection with 100% probability, therefore the surviving probability of EPR states are also $p_1 = (1 - \frac{3p}{4})^n$.
2. EPR states affected by Z errors: This kind of state can survive the error detection if Z -errors happen in the $n - m$ qubits while the m qubits being measured is of pure EPR states. Therefore the probability of these kinds of state left is $p_2 = (1 - \frac{3p}{4})^m \left((1 - \frac{p}{2})^{n-m} - (1 - \frac{3p}{4})^{n-m} \right)$.
3. EPR states also affected by X errors: This kind of state pass the error detection with probability only 2^{-m} . Therefore the overall surviving probability of them after error detection is $p_3 = 2^{-m} \left(1 - (1 - \frac{p}{2})^n \right)$.

Now we calculate the bit and phase error rate of the surviving $n - m$ qubits after error detection. Denote \bar{e}_b the average bit error rate over states that are affected by X -errors before distillation. Since overall bit error rate is $p/2$ before distillation for local depolarizing noise, we should have

$$\frac{\bar{e}_b \left(1 - (1 - \frac{p}{2})^n \right) + 0 \cdot (1 - \frac{p}{2})^n}{\left(1 - (1 - \frac{p}{2})^n \right) + (1 - \frac{p}{2})^n} = p/2 \Rightarrow \bar{e}_b = \frac{p}{2 \left(1 - (1 - \frac{p}{2})^n \right)}. \quad (\text{B52})$$

After suppression of X error, the remaining bit error rates are

$$\begin{aligned} e_b &= \frac{2^{-m} \bar{e}_b \left(1 - (1 - \frac{p}{2})^n \right)}{2^{-m} \left(1 - (1 - \frac{p}{2})^n \right) + (1 - \frac{3p}{4})^m (1 - \frac{p}{2})^{n-m}} \\ &= \frac{1}{1 - (1 - \frac{p}{2})^n + 2^m (1 - \frac{3p}{4})^m (1 - \frac{p}{2})^{n-m}} \cdot \frac{p}{2} \\ &= \frac{1}{1 + (1 - \frac{p}{2})^{n-m} \left((2 - \frac{3p}{2})^m - (1 - \frac{p}{2})^m \right)} \cdot \frac{p}{2}. \end{aligned} \quad (\text{B53})$$

To require the bit error to be exponentially suppressed. We first need $(2 - \frac{3p}{2})^m - (1 - \frac{p}{2})^m > 0$. This is trivially true because $2 - \frac{3p}{2} > 1 - \frac{p}{2}$ whenever $p < 1$. Then what is required is that $(1 - \frac{p}{2})^{n-m} (2 - \frac{3p}{2})^m$ is exponentially large. This can be achieved in the large n limit as long as $(1 - \frac{p}{2})^{1-\frac{m}{n}} (2 - \frac{3p}{2})^{\frac{m}{n}} = 1 + \delta$ for any small constant $\delta > 0$. Then the solution p_{tol} to equation $(1 - \frac{p}{2})^{1-\frac{m}{n}} (2 - \frac{3p}{2})^{\frac{m}{n}} = 1$ serves as the maximal tolerable noise strength because, in the large n limit, when bit error is exponentially suppressed, the protocol could tolerate any phase error $e_p < \frac{1}{2}$ since $1 - H(e_p) > 0$ for any $e_p < \frac{1}{2}$.

Now we consider the phase error rate to complete the proof for key rate. For pure EPR states and EPR states affected only by Z -errors, the average phase error rate is

$$\begin{aligned} \bar{e}_p &= \Pr\{Z\text{-error} \mid \text{no } X \text{ or } Y \text{ error}\} \\ &= \frac{\Pr\{Z\text{-error}, \text{ no } X \text{ or } Y \text{ error}\}}{\Pr\{\text{no } X \text{ or } Y \text{ error}\}} \\ &= \frac{p/4}{1 - p/2}. \end{aligned} \quad (\text{B54})$$

Note that after diagonal twirling, those surviving EPR pairs with X -errors would have $1/2$ phase error rate due to the complete dephasing channel. Therefore the overall phase error is:

$$e_p = \frac{\frac{p/4}{1-p/2} (1 - \frac{3p}{4})^m (1 - \frac{p}{2})^{n-m} + \frac{1}{2} \cdot 2^{-m} (1 - (1 - \frac{p}{2})^n)}{(1 - \frac{3p}{4})^m (1 - \frac{p}{2})^{n-m} + 2^{-m} (1 - (1 - \frac{p}{2})^n)}. \quad (\text{B55})$$

Since bit error is exponentially suppressed. After measuring all pairs in the computational basis, no bit error correction is needed. To generate secure keys, the QKD protocol only requires a privacy amplification step with output ratio $1 - H(e_p)$. Therefore the overall key rate is

$$R = \left(\left(1 - \frac{3}{4}p\right)^m \left(1 - \frac{p}{2}\right)^{n-m} + 2^{-m} \left(1 - \left(1 - \frac{p}{2}\right)^n\right) \right) (1 - H(e_p)) (1 - m/n). \quad (\text{B56})$$

□

Appendix C: Simulation setup for quantum key distribution and repeaters

Following [39], we choose parameter from some of the most recent experiments [38, 44, 45]. Important parameters for simulation includes: Average bit error rate for nonzero photon components e_d , defined to be the bit error rate for photons in a channel. We will choose this to be the varying factor in QKD simulation. In repeater this is set to $e_d = 1.5\%$; Phase-noise accumulation rate $\beta = 2.82 \times 10^{-4} \text{km}^{-1}$, defined as the rate of dephasing channel strength accumulated through distance; Dark count rate $Y_0 = 3 \times 10^{-8}$, defined as the probability of obtain a click when there is no photon in the channel; Optical fiber loss $\alpha = 0.21$, defined as the coefficient such that the transmittance η over fibres of length l kilometers is $\eta = 10^{-\alpha l/10}$; error correction efficiency $f = 1.06$, which is the overhead factor of key rates in bit error correction.

Here for simplicity, we assume that we have ideal single photon source or have an ideal photon-number-resolving device such that it can filtered out all multiple-photon components. Note that even these two very ideal assumption are becoming increasingly realistic with the advancements in single-photon source and detector technology [46]. In this scenario, we could focus on the single photon case corresponding to the qubit system. The dark count could be understood as the state is loss during transmission but a maximally-mixed state occurs from the channel prohibiting us from really knowing that the EPR state is lost. Therefore the corresponding error rates when dark count event happens is $1/2$. The total bit error rate for a single photon is thus,

$$e_b = \frac{\eta e_d + \frac{1}{2}(1 - \eta)Y_0}{\eta + (1 - \eta)Y_0}, \quad (\text{C1})$$

where $\eta = 10^{-\alpha l/10}$ decays exponentially with distance. The phase of quantum states are more fragile during the transmission, we model the phase error by another independent dephasing channel with strength [38],

$$p = \frac{1 - e^{-\beta l/2}}{2}, \quad (\text{C2})$$

here l is the transmission distance. The value of β is taken also from [38], modeling their residual phase noise remained after active fibre phase-noise suppression. Taking the dark count into account, the overall phase error rate is therefore,

$$e_p = \frac{\eta(1 - e^{-\beta l/2})/2 + \frac{1}{2}(1 - \eta)Y_0}{\eta + (1 - \eta)Y_0}. \quad (\text{C3})$$

For QKD, the maximum transmission distance is obtained when the net key rate

$$R_{\text{one}} \propto 1 - fH(e_b) - H(e_p) \leq 0. \quad (\text{C4})$$

Here $H(e)$ is the Shannon entropy. We add an error correction efficiency factor f to one of such entropy to represent the additional overhead by the error correction step. For two way protocols with recurrence method, we first compute the bit error rate e'_b and phase error rate e'_p after given rounds of recurrence. Then, similiary, the maximum transmission distance is given by the point where

$$R_{\text{two}} \propto 1 - fH(e'_b) - H(e'_p) \leq 0. \quad (\text{C5})$$

For Hamiltonian-based protocol, we choose a 15-qubit diagonal Hamiltonian and measure 12 qubits in the Hadamard basis. Since here we are working with finite Hamiltonian. Even though the bit error rate is still significantly suppressed, we cannot directly overlook it as done in the proof of Theorem 4. We calculate the bit error rate and phase error rate e_b^H, e_p^H using Eq. (B53) and Eq. (B55). Similarly the maximum transmission distance is determined when

$$R_{\text{H}} \propto 1 - fH(e_b^H) - H(e_p^H) \leq 0. \quad (\text{C6})$$

For repeaters, we directly calculate the bit and phase error rate and then report the fidelity, both without distillation and that after two-way distillation methods including recurrence method or Hamiltonian-based method.